UNIVERSITY OF THESSALY
Department of Civil Engineering

UNIVERSITE JOSEPH FOURIER
Observatoire des Sciences de l'Univers de Grenoble

AN INVESTIGATION OF URBAN HEAT ISLAND INTENSITY (UHII) USING REMOTE SENSING AND LAND COVER CLASSIFICATION TECHNIQUES. A CASE STUDY FOR LARISSA, GREECE.

M.Sc. Management of Hydrometeorological Hazards – HYDROHASARDS

Master thesis submitted by

***K.Koumantzelis*[1]**

Supervised by

Dr. Marios Spiliotopoulos

(1) Department of Civil Engineering, University of Thessaly, Pedion Areos, Volos, 38333,Greece
e-mail: kkoumantz@hotmail.gr

January 2016

ACKNOWLEDGEMENTS

I would like to thank Dr. Marios Spiliotopoulos for creating and entrusting this subject to me and for the invaluable help and guidance he provided throughout the study.
I wish to thank in general all the teaching staff at UJF and at the University of Thessaly that participated in the MSc of Hydrohazards for the knowledge that I acquired.
I would also like to extend my deepest gratitude to my family for their constant moral support and love.
This work was made possible to a large degree due to the USGS policy, by making their source code open and free of charge.
Finally, I would like to thank my beloved Dimitra Plitsi, Civil Engineer and M.Sc. in Hydraulics for all the scientific help that she provided to me.

GLOSSARY

Atmospheric Heat Islands	AHI
Advanced Spaceborne Thermal Emission and Reflection Radiometer	ASTER
Advanced Very High Resolution Radiometer	AVHRR
Boundary Layer Heat Island	BLHI
Classification-Based Emissivity Method	CBEM
COoRdinate INformation on the Environment	Corine
Corine Land Cover	CLC
Canopy Layer Heat Island	CLHI
Commercial/Industrial	C/I
Digital Number	DN
European Environment Agency	EEA
Enhanced Thematic Mapper Plus	ETM+
Ground Control Points	GCP
Greek Geodetic Reference System	GGRS
Geographic Information Systems	GIS
Hellenic National Meteorological Service	HNMS
Intergovernmental Panel on Climate Change	IPCC
Land Surface Emissivity	LSE
Land Surface Temperature	LST
Land-Use/Land-Cover	LULC
Landsat 8	L8
Maximum Likelihood	M-L
Multi-mission Modular Spacecraft	MMS
Moderate Resolution Imaging Spectroradiometer	MODIS
Multispectral Scanner	MSS
NDVI-based emissivity method	NBEM
Normalized Difference Vegetation Index	NDVI
Normalized Difference Water Index	NDWI
National Observatory of Athens	NOA
Operational Land Imager	OLI

Return Beam Vidicon	RBV
Root Mean Square	RMS
Scan Line Corrector	SLC
Surface Urban Heat Island	SUHI
Short-wave Infrared	SWIR
Temperature Emissivity Separation	TES
Thermal InfraRed Sensor	TIRS
Top Of Atmosphere	TOA
Urban Heat Island Intensity	UHII
United States Environmental Protection Agency	US EPA
United States Geological Survey	USGS
USGS Earth Resources Observation and Science	USGS EROS
University Joseph Fourier	UJF
University of Thessaly	UTH
Vegetation Fractional Cover	VFC
Visible Near InfraRed	VNIR
World Wildlife Fund	WWF

ABSTRACT

The aim of this study is to investigate the Intensity of Urban Heat Island (UHII) in the city of Larissa, capital of Thessaly region, in Greece. For this purpose Landsat 8 images were used for the retrieval of Normalized Difference Vegetation Index (NDVI) and Land Surface Emissivity (LSE) so as to derive Land Surface Temperature (LST). The correlation between LST values and maximum temperature values measured by meteorological stations was efficient and the retrieved function was applied to a new image, for validation of LST values. The UHII was estimated by applying a polygon summary Geographical Information Systems (GIS) operation using LST values, in combination with urban land cover information provided by the Corine land cover (CLC) database. The results were compared to two kinds of land cover classification technique. Finally, the correlation among NDVI, LST and Vegetation Fractional Cover (VFC) was retrieved.

Keywords: Remote Sensing; Normalized Difference Vegetation Index; Urban Heat Island; Land Surface Temperature; Land Cover Classification

ΠΕΡΙΛΗΨΗ

Ο σκοπός αυτής της μελέτης είναι να διερευνήσει την ένταση της Αστικής Θερμικής Νησίδας (UHII) στην πόλη της Λάρισας, πρωτεύουσα της περιφέρειας Θεσσαλίας, στην Ελλάδα. Γι 'αυτό το σκοπό Landsat 8 εικόνες χρησιμοποιούνται για την εύρεση του κανονικοποιημένου δείκτη βλάστησης (NDVI) και της ακτινοβολίας στην επιφάνεια της γης (LSE), έτσι ώστε να εκτιμήσουμε τη θερμοκρασία στην επιφάνεια της γης (LST). Η συσχέτιση μεταξύ τιμών θερμοκρασίας βασιζόμενων σε δορυφόρο (LST) και θερμοκρασίας που μετράται από μετεωρολογικούς σταθμούς ήταν ικανοποιητική και η συνάρτηση συσχέτισης που προέκυψε, χρησιμοποιήθηκε σε μια νέα εικόνα, για επικύρωση των τιμών επιφανειακής θερμοκρασίας (LST). Η UHII εκτιμήθηκε εφαρμόζοντας μέθοδο χρήσης πολύγωνου στο Σύστημα Γεωγραφικών Πληροφοριών (GIS), χρησιμοποιώντας τιμές LST, σε συνδυασμό με την αστική πληροφορία χρήσεων γης που παρέχεται από τη βάση δεδομένων εδαφοκάλυψης Corine (CLC). Τα αποτελέσματα συγκρίθηκαν με δύο είδη τεχνικής ταξινόμησης χρήσεων γης. Τέλος, υπολογίστηκε η συσχέτιση μεταξύ NDVI, LST και της κλασματικής κάλυψης βλάστησης (VFC).

Λέξεις-κλειδιά: Τηλεπισκόπηση, Κανονικοποιημένος Δείκτης Βλάστησης, Αστική Θερμική Νησίδα, Επιφανειακή Θερμοκρασία, Ταξινόμηση Χρήσεων Γης

RESUME

Le but de cette étude est d'étudier l'intensité de l'île de chaleur urbain (ICUI) dans la ville de Larissa, capitale de la région de Thessalie, en Grèce. A cet effet Landsat 8 images ont été utilisées pour la récupération de l'Indice de Végétation Différence Normalisée (NDVI) et l'émissivité de la surface terrestre (LSE) de manière à dériver Température de la surface terrestre (HNL). La corrélation entre les valeurs de LST et

les valeurs de température maximale mesurée par les stations météorologiques a été efficace et la fonction récupéré appliqué à une nouvelle image, pour la validation de valeurs LST Le UHII a été estimé en appliquant un résumé de polygone géographique dans ArcMap environnement GIS en utilisant les valeurs LST, en combinaison avec l'information urbaine de la couverture terrestre fournies par la base de données Corine Land Cover (CLC). Les résultats ont été comparés à deux types de technique de classification de la couverture terrestre. Enfin, l'ampleur de corrélation entre NDVI, LST et Végétation Fractional Cover (VFC) a été récupéré.

Mots-clés: Télédétection; Indice de Végétation Différence Normalisée; Îlot de Chaleur Urbain; Terrain Température de la Surface; Classification de la Couverture Terrestre

CONTENTS

1 INTRODUCTION

1.1 UHI phenomenon

The UHI refers to the phenomenon of higher atmospheric and surface temperatures occurring in urban areas than in the surrounding rural areas due to urbanization (Voogt and Oke, 2003). It is characterized by a large expansion of non-evaporating impervious materials covering a majority of urban areas with a consequent increase in sensible heat flux at the expense of latent heat flux (Oke, 1982; Owen et al., 1998). UHI effects are intensified by the anthropogenic heat generated by traffic, industry and domestic buildings, impacting the local climate through the city's compact mass of buildings that affect exchange of energy and levels of conductivity. The higher temperatures in urban heat islands increase air conditioning demands, raise pollution levels, and may modify precipitation patterns. As a result, the magnitude and pattern of UHI effects have been major concerns of many urban climatology studies (Yuan & Bauer, 2006).

The UHI phenomenon was first mentioned in 1820 by Luke Howard, who after investigation, compared the temperature data within London and the suburban area, and concluded an "artificially increasing heat" in the city in relation to its surroundings (Howard, 1833). During the 19th century, Renou (Renou, 1855; Renou, 1862; Renou, 1868) made similar findings for Paris and in the 20th century, Wilhelm Schmidt for Vienna (Schmidt, 1917; Schmidt, 1929). The studies of the phenomenon in the United States of America began in the 20th century (Mitchell, 1953; Mitchell, 1961). Regarding Greece, the existence of UHI phenomenon in Athens, had already been confirmed by relevant climatological studies carried out in the early 1980s (Katsoulis and Theoharatos, 1985). Since then, the characteristics of the UHI effects in Athens have been the focus of numerous studies based both on ground observations (Santamouris et al., 1999; Mihalakakou et al., 2002; Livada et al., 2002; Mihalakakou et al., 2004; Kassomenos and Katsoulis, 2006; Repapis et al., 2007; Giannopoulou et al., 2011; Giannaros et al., 2013) and satellite observations (Stathopoulou and Cartalis, 2007; Stathopoulou et al., 2009).

1.1.1 Types of UHI

Heat islands can be characterized for different layers of the urban atmosphere and for various surfaces and divided into three categories: canopy layer heat island (CLHI), boundary layer heat island (BLHI), and surface urban heat island (SUHI). The urban canopy layer extends upwards from the surface to approximately mean building height, whereas the urban boundary layer is located above the canopy layer (Voogt and Oke, 2003). The CLHI and the BLHI are atmospheric heat islands (AHI) since they denote a warming of the urban atmosphere, whereas the SUHI refers to the relative warmth of urban surfaces compared to surrounding rural areas. It is known that atmospheric UHIs are larger at night while surface UHIs are larger during the day (Roth et al, 1989). While AHIs are measured by in situ sensors of air temperature via weather station networks, the SUHI is typically characterized as land surface temperature (LST) through the use of airborne or satellite thermal infrared remote sensing, which provides

a synoptic and uniform means of studying SUHI effects at regional scales (Liu et al, 2005).

Satellite thermal data can effectively depict the patterns of the thermal environment of extensive urban areas on a repeated basis. Thus, spatial coverage and temporal repetition are the main advantages of using satellite thermal remote sensing technique in the study of the urban climates (Stathopoulou and Cartalis, 2007).

Table 1.1: Basic characteristics of SUHI and AUHI (Adapted from United States Environmental Protection Agency (EPA), 2014)

Feature	Surface UHI	Atmospheric UHI
Temporal Development	• Present at all times of the day and night • Most intense during the day and in the summer	• May be small or non-existent during the day • Most intense at night or predawn and in the winter
Peak Intensity (Most intense UHI conditions)	• More spatial and temporal variation: ▪ Day: 18 to 27°F (10 to 15°C) ▪ Night: 9 to 18°F (5 to 10°C)	• Less variation: ▪ Day: -1.8 to 5.4°F (-1 to 3°C) ▪ Night: 12.6 to 21.6°F (7 to 12°C)
Typical Identification Method	• Indirect measurement: ▪ Remote sensing	• Direct measurement: ▪ Fixed weather stations ▪ Mobile traverses
Typical Depiction	• Thermal image	• Isotherm map • Temperature graph

1.1.2 Remote Sensing in UHI detection

The utilization of remote sensing in the assessment of surface thermal properties as well as surface UHI has been carried out by various researchers (Artis and Carnahan, 1982; Roth, 1989; Nichol, 1994; Xue and Cracknell, 1995; Carlson et al., 1997; Owen, 1998; Santamouris et al., 2001; Streutker, 2002; Dousset and Gourmelon, 2003; Lo and Quattrochi, 2003; Stathakis, 2003; Voogt and Oke, 2003; Sobrino et al., 2004; Stathopoulou et al., 2005; Chen et al., 2006; Jiménez-Muñoz et al., 2006; Xian and Crane, 2006; Yuan and Bauer, 2006; Santana, 2007; Stathopoulou and Cartalis, 2007; Sun and Kafatos, 2007; Yuan and Bauer, 2007; Yue et al., 2007; Fortuniak, 2009; Aniello et al., 2010; Arrau and Pena, 2010; Su et al., 2010; Perakis, 2011; Stathopoulou and Cartalis, 2011; Hoyos, 2014; Orhan et al., 2014; Yu et al., 2014; Liu et al., 2015).

These studies can be conducted using satellite sensors such as Moderate Resolution Imaging Spectroradiometer (MODIS) and Advanced Very High Resolution Radiometer (AVHRR), which have been found to be feasible to describe the coarse thermal spatial distributions, yet, insufficient to investigate the accurate relationships between LST and surface characteristics. On the other hand, satellite sensors of medium spatial resolution,

such as Landsat Thematic Mapper (TM)/Enhanced Thematic Mapper Plus (ETM+) thermal infrared data and ASTER (Advanced Spaceborne Thermal Emission and Reflection Radiometer), have been extensively utilized for studies of SUHI at the local scale. For example, Stathopoulou and Cartalis in 2011, used ETM images to assess the thermal environment of major cities in Greece; Chen, et al. in 2006, examined the changes in Land Cover Types and the associated intensity and spatial pattern of the SUHI effect in a rapidly changing area of the Pearl River Delta region in China (Liu et al., 2015).

1.2 Objectives of the study

The main objective of the study is the estimation of UHII in Larissa region by using Landsat-8 thermal images of high spatial resolution (≤ 100m) related to 6 different summer months. Moreover, as it is presented in Chapter 3, a validation check is utilized for LST values, through correlation analysis between maximum air temperature values measured in 6 different dates provided by 14 different stations and satellite retrieved surface temperature values, resulted from the production of 105 maps.

The significance of the study presented here lies, not only in applying Landsat-8 images for the first time in Larissa city through an important, widespread and not complicated method for estimating the UHII, but also in the applicable prospect of creating time-series of temperature values, retrieved by satellite images. In addition, time-series of air temperature values, with missing data from stations, could be filled by estimating LST values. For a deeper investigation of the UHII retrieval process, a comparison of three different approaches is performed, revealing the efficiency of polygon summary approach for this specific goal, compared to unsupervised isocluster and supervised maximum likelihood classification techniques.

Another aim is to investigate the presence and magnitude of negative correlation between LST - NDVI, as well as LST - VFC, so as to extract useful conclusions about the interplay between vegetation cover and UHII. The findings can contribute to the proposal of urban planning and water resource measures by policy makers, focused on UHI reduction and the adaptation of cities to the challenges of climate change.

1.3 Outline of the study

The study is organized as follows: Chapter 2 describes the study area and the data set that was used in the study. It also contains a brief theoretical background about the UHI phenomenon; Chapter 3 explains the methodology framework, the theory and the tools that were used in this study, along with some first and basic results. Specifically it includes information about the image pre-processing, the retrieval of at-satellite brightness temperature, the method that was followed for finding land surface emissivity, the process regarding the land surface temperature estimation. In addition, it consists of the correlation – validation procedure of LST, a first investigation of correlation between NDVI, VFC and LST as well as the estimation of UHII through two main approaches; Chapter 4 presents more profoundly and discusses the results of the above-mentioned and Chapter 5 holds the conclusions.

2 BACKGROUND

2.1 Spatial characteristics of the UHI

The spatial characteristics of the UHI are contingent upon the configuration and topographic setting of the urban area, however, the spatial pattern of UHI isotherms are typically aligned with the urban-rural boundary (Voogt, 2002). Moreover, the increased temperatures associated with the UHI phenomenon are not uniform across the urban area as whole, as intra-urban thermal patterns are generally influenced by urban surface features (Santana, 2007). A sketch of a typical UHI profile is provided in Figure 2.1.

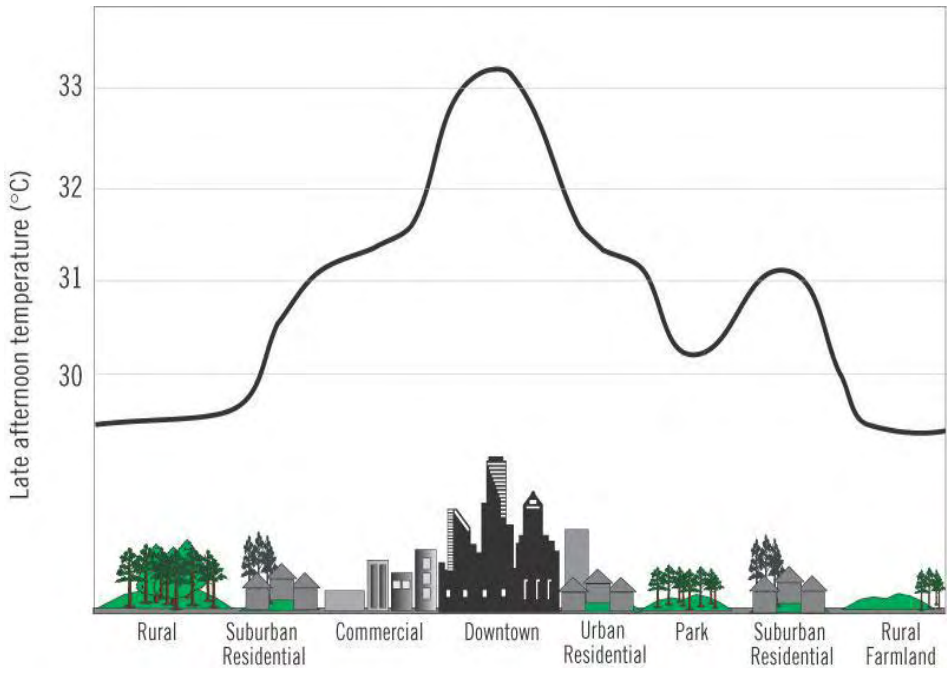

Figure 2.1: Sketch of a typical UHI profile. (Adapted from Arrau and Pena, 2010).

2.2 UHII

The intensity of an UHI is known as UHII, which can be defined as the air temperature difference between urban and rural areas. UHII is influenced by climate region, local topography, industrial development of a city (Stathopoulou et al., 2005) city size and density, Land-Use/Land-Cover (LULC) characteristics, the characteristics of the surrounding rural areas (Fortuniak, 2009) and vegetation abundance (Santana, 2007). Meteorological conditions (especially wind speed and cloud cover) and sun intensity also influence the development of the UHI – and therefore, UHII tends to vary both hourly and seasonally (EPA, 2009a). Of all the factors mentioned above, LULC characteristics and the abundance of urban vegetation are the two factors which are

considered to have the most significant effect on UHI intensity, as well as on intra-urban thermal patterns (Xian and Crane, 2006; Arrau and Pena, 2010).

2.3 Surface and Air Temperatures

LSTs are considered to be a reliable indicator of the UHI as there is generally a high correlation between LSTs and air temperatures in the canopy layer, due to the transfer of thermal energy emitted from the surface to the atmosphere (Nichol, 1994; Arrau and Pena, 2010). However, due to the fact that air mixes within the atmosphere, the relationship between surface and near-surface air temperatures is not constant (EPA, 2009a). As can be observed in Figure 2.2, atmospheric temperatures normally fluctuate less than surface temperatures across a given area during the day, while a more congruent relationship between atmospheric and surface temperatures can be observed during the nighttime hours (Farina, 2012).

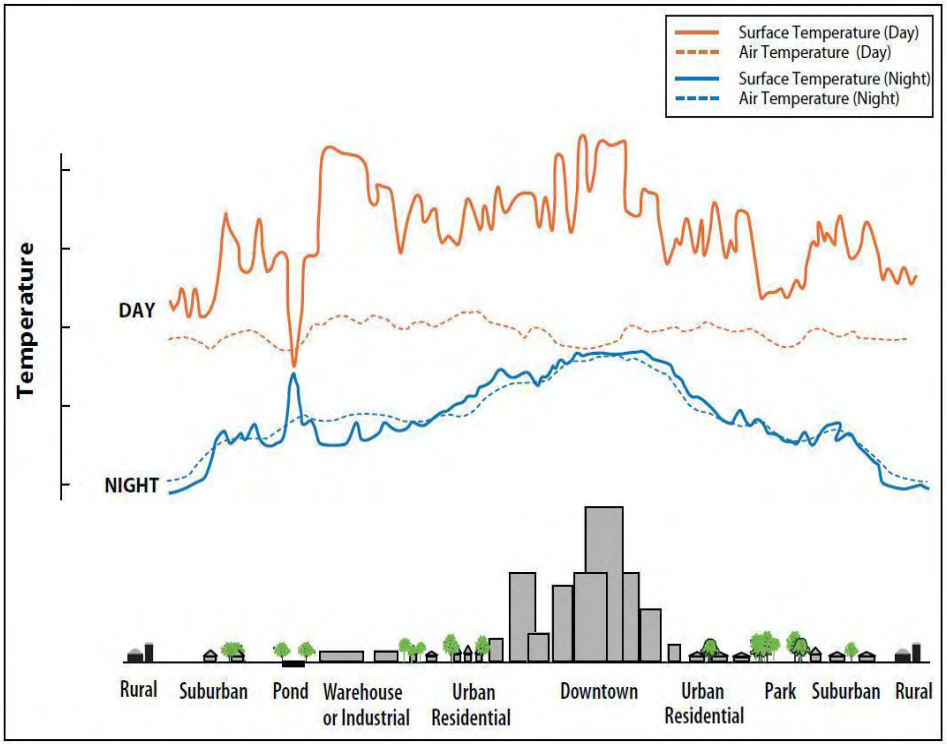

Figure 2.2: Variations in Atmospheric and Surface temperatures. (Adapted from EPA, 2009a).

2.4 Environmental and Social Impacts of UHII

Although there may be certain positive impacts attributable to the increased temperatures associated with UHIs (including the melting of ice on roads during the winter, reductions in energy required for heating, and longer plant-growing season), such potential benefits are largely outweighed by the substantial detrimental

environmental and social aspects discussed below (EPA, 2009a). Especially in cities with hot climate, the phenomenon of urban heat island has significant negative impacts on energy and water consumption, air quality, in public health but also to the feeling of thermal comfort of city residents (Stathopoulou and Cartalis, 2011).

2.4.1 Increased energy consumption and greenhouse gasses

The increased temperatures associated with the UHI are known to have major negative environmental impacts, not only on urban environments but also on ecosystems in rural areas (Arrau and Pena, 2010). In fact, UHIs can contribute, in an indirect manner, to climate change as elevated summertime temperatures in cities often result in the need for increased energy consumption due to a higher demand for air conditioning. This, in turn, often requires increased use of fossil-fuel powered plants, increasing emissions of greenhouse gases such as Carbon Dioxide (CO_2) into the atmosphere (Santana, 2007; EPA, 2009b). Urban electricity demands are known to rise on average 1.5 to 2% for every 0.6°C increase in air temperatures, starting from about 20 to 25°C (EPA, 2009b). One study showed that, within the United States, 5-10% of urban peak electricity demand is used to compensate for the UHI effect (Akbari, 2005). Another research in Athens by Santamouris revealed that the increased energy demand for air conditioning leads to additional peak load, which requires huge investments to build new power stations. These new channels are necessary in accordance with the current data for use during the summer while the remainder are underperforming as demand decreases rapidly. The result is the increased cost of producing a per kWh in consequence of the use of these substations that can touch up 62% increase in the average cost of production (Santamouris, 2001).

2.4.2 Air quality

In addition to greenhouse gas emissions, the increase in energy demand associated with elevated summer temperatures also often results in higher levels of air pollution as fossil-fuel powered plants (which currently provide about 66% of global electricity) emit Nitrogen Oxides (NOx), Mercury (Hg), Carbon Monoxide (CO), Sulfur Dioxide (SO_2), and Particulate Matter (PM) into the atmosphere (EPA, 2009a; WWF, 2010). These pollutants are known to have a detrimental effect on air quality, contributing to acid rain and other phenomena which may be harmful to human health. Higher urban temperatures are also known to increase ground-level ozone, which is the result of a reaction between Organic Compounds (VOCs) and NOx (Santana, 2007; EPA, 2009a).

2.4.3 Water quality

The high temperatures of city sidewalks and roofs can heat rainwater. According to studies in sidewalks, whose temperature was 38 °C, an increase in rainwater temperature was detected from about 21 ° C to 35 ° C. The warm rainwater gathering to network storm and reaching streams, rivers, and lakes increase the temperature (Zisopoulou and Kasdaglis, 2011). The water temperature affects all aspects of aquatic life, especially the metabolism and reproduction of many aquatic species. Rapid temperature changes in aquatic ecosystems resulting from rainwater runoff can be fatal to aquatic life (US EPA, 2008).

2.4.4 Increased instability of the urban atmosphere

According to (Parry et al. 2007) the UHI phenomenon reduces the stability of the urban atmosphere at night which, under certain meteorological conditions, may intensify the development of convective clouds. Therefore, the effect of rainfall events (which according to the Intergovernmental Panel on Climate Change (IPCC) are expected to increase in magnitude and frequency due to climate change) may be amplified in urban areas, resulting in economic losses and extra costs due to, among other things, the need for improvements in storm-water drainage (Parry et al. 2007; Fortuniak, 2009).

Another phenomenon associated with the urban heat island is the inversion temperature, as it is called the state of the atmosphere in which the temperature of the air inside a layer of the troposphere increases with the height, rather than declining, as usually happens under normal conditions. Hot air rises over the city, meets the reversal, and spreads sideways. As it moves, partial radiates from its own heat. This radiation cools the air, increasing its density, resulting in the wind to subside over the countryside just beyond the city limits. From there it flows back to the city, in the area of low pressure at Centre. There is thus a convergence in the inner part of the city and cast over the city, and warm air below the inversion has roughly dome-shaped figure (Boudas, 2014).

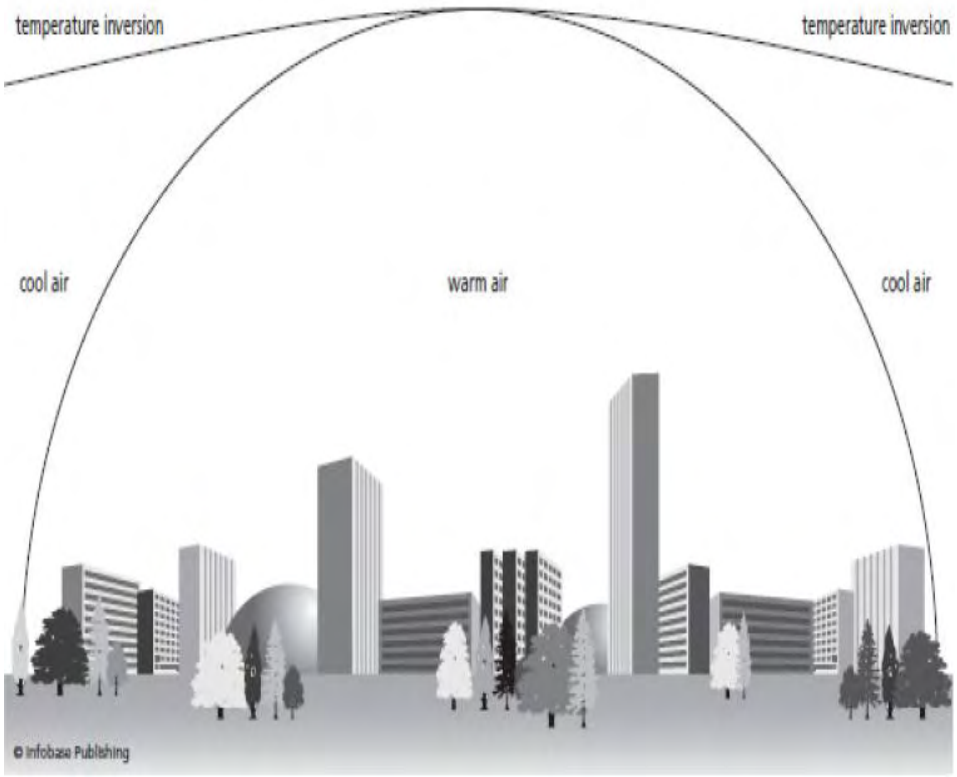

Figure 2.3: Temperature inversion effect (Allaby, 2007).

2.4.5 Human health

Since UHIs tend to exacerbate the impact of heat waves, heat-related fatalities are another consequence of increased urban temperatures (Fig. 2.4), (EPA, 2009a). For example, the 2003 heat wave over Europe caused an estimated 35,000 fatalities (Gill et al., 2007). Due to the UHI, temperatures during heat waves often do not cool off significantly during the night. High nighttime temperatures during heat waves are associated with increased mortality even more so than high daytime temperatures since there is no break from the heat, giving people no significant relief (Kalkstein, 1991). In addition to heat-related mortality, increased urban temperatures may also contribute to heat cramps, exhaustion, non-fatal heat stroke and general discomfort (EPA, 2009a). Climate change is expected to intensify such impacts, as current climate change models predict a general increase in summer temperatures and longer durations of heat waves (Gill et al., 2007).

2.4.6 Socio-economic aspect

According to a study of Santamouris M. in 2001, regarding the city of Athens, UHI phenomenon presents also significant economic implications. The problem lies mainly in populations with low annual incomes, who live in areas of central and western suburbs, where the temperature is too high in relation to the northern suburbs. The

majority of buildings which house these populations, are characterised by "energy losses" (without insulation, double glazing etc.), while at the same time cannot afford energy upgrade. The combination of elevated external temperatures during the summer season and energy "weak" buildings, results in twice the energy consumption for air conditioning. Therefore the purchase of thermal comfort for these low-income groups has much higher costs than populations with moderate or high income (Santamouris M., 2001).

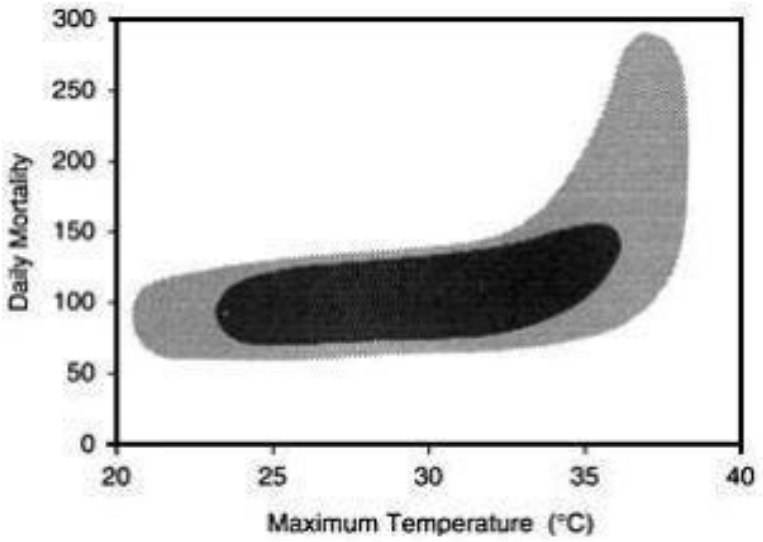

Figure 2.4: Relationship between mortality and maximum atmospheric temperature in Shanghai (1980 to 1989).

In Fig. 2.4 is notable that at temperatures above 34 ºC there is a marked increase in heat-related deaths. Shading is based upon density of data points. (Source: Oke, 1997; data adapted from the original research by Kalkstein and Smoyer, 1993).

2.5 Study Area

Larissa, which has been chosen as the area of study for UHII, is the capital and largest city of the Thessaly region of Greece. It is a principal agricultural centre and a national transportation hub, linked by road and rail with the port of Volos, the city of Thessaloniki and Athens. Larissa, within its municipality, has 162,591 inhabitants, while the regional unit of Larissa reached a population of 284,325 in 2011 (Hellenic Statistical Authority). The area of the city is characterized by 67 m. mean elevation extending over an area of 122.6 km^2. Although mostly contained within the Larissa municipality, also includes the communities of Giannouli, Platykampos, Nikaia, Terpsithea and several other suburban settlements, bringing the wider urban area population of the city to 174,012 inhabitants and extends over an area of 572.3 km^2. Larissa lies on the river Pineios, and the northern part of its regional unit is covered with forests, but most of it, is fertile land, the Thessalian Plain. The climate in Larissa is

classified as Csa by the Köppen - Geiger system. The average annual temperature is 15.6 °C and about 468 mm of precipitation falls annually (http://en.climate-data.org). The winter is cold and wet, and some snowstorms may occur. The summer is hot, and temperatures of 40 °C (104 °F) may occur. Thunderstorms or heavy rain may cause agricultural damage and is the largest city in Greece, among those cities which present very high summer temperatures (www.wikipedia.org). There are many meteorological stations in the country that record temperatures exceeding 40 degrees Celsius but none beside a city of around 170,000 inhabitants. The station of Hellenic National Meteorological Service in Larissa is of 3 km distance from the city center, and is considered to be among the 3-4 warmest in the whole country (www.e-meteolarissa.blogspot.gr).

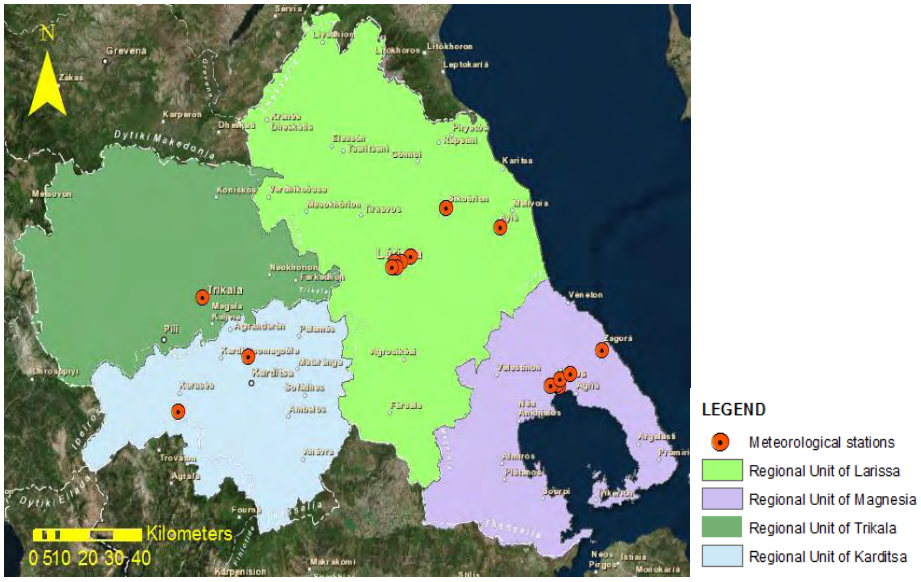

Figure 2.5: Thessaly region and the depicted meteorological stations that are used in the correlation – validation process of LST.

2.6 Satellite and Field Data

84 scenes of 7 Landsat8 images were initially downloaded from the U.S Geological Survey (USGS) Earth Explorer Website. The dates of the images that were chosen initially for the study were: 27/06/2014, 13/07/2014, 14/08/2014, 14/06/2015, 16/07/2015, and 17/08/2015. As it will be mentioned in details below, a validation-image of 01/08/2015 was also downloaded and utilized. Every satellite image which was acquired from the USGS was captured at approximately 12:00 a.m. local time under quite sufficiently clear atmospheric conditions. The cloud coverage ranged by 0.19 (14/08/2014) to 9.79 % at 17/08/2015 image.

Landsat satellites have been providing multispectral images of the Earth continuously since the early 1970's. Landsat data have been utilized in a variety of government, public, private, and national security applications. Examples include land and water management, global change research, oil and mineral exploration, agricultural

yield forecasting, pollution monitoring, land surface change detection, and cartographic mapping. Landsat 8 is the latest satellite in this series. The first was launched in 1972 with two Earth-viewing imagers - a return beam vidicon (RBV) and an 80-meter 4-band multispectral scanner (MSS). Landsat 2 and 3, launched in 1975 and 1978 respectively, were configured similarly. In 1984, Landsat 4 was launched with the MSS and a new instrument called the Thematic Mapper (TM). Instrument upgrades included improved ground resolution (30 meters) and 3 new channels or bands. In addition to using an updated instrument, Landsat 4 made use of the multi-mission modular spacecraft (MMS), which replaced the Nimbus based spacecraft design employed for Landsats 1-3. Landsat 5, a duplicate of Landsat 4, was launched in 1984 and returned scientifically viable data for 28 years - 23 years beyond its 5-year design life. Landsat 6, equipped with an additional 15-meter panchromatic band, was lost immediately after launch in 1993. Landsat 7 was launched in 1999 and performed nominally until its scan line corrector (SLC) failed in May 2003. Since that time, Landsat 7 continues to acquire to this day useful image data in the "SLC off" mode. All Landsat 7 SLC-off data are of the same high radiometric and geometric quality as data collected prior to the SLC failure. Landsat 8 (L8) was launched in February 11, 2013 and its mission objective is to provide timely, high quality visible and infrared images of all landmass and near-coastal areas on the Earth, continually refreshing the existing Landsat database. Data input into the system is sufficiently consistent with currently archived data in terms of acquisition geometry, calibration, coverage and spectral characteristics to allow for comparison of global and regional change detection and characterization (LANDSAT 8 (L8) DATA USERS HANDBOOK, 2015). Compared to previous edition, L8 Operational Land Imager (OLI) and Thermal Infrared Sensor (TIRS) images consist of nine spectral bands with a spatial resolution of 30 meters for Bands 1 to 7 and 9. New band 1 (ultra-blue) is useful for coastal and aerosol studies. New band 9 is useful for cirrus cloud detection. The resolution for Band 8 (panchromatic) is 15 meters. Thermal bands 10 and 11 are useful in providing more accurate surface temperatures and are collected at 100 meters. Approximate scene size is 170 km north-south by 183 km east-west.

Table 2.1: Spectral and spatial resolution characteristics of Landsat 8 bands used in the research (adapted from landsat.usgs.gov/band_designations_landsat_satellites.php).

Bands	Wavelength (μm)	Resolution (m)
Band 1 - Coastal aerosol	0.43 - 0.45	30
Band 2 - Blue	0.45 - 0.51	30
Band 3 - Green	0.53 - 0.59	30
Band 4 - Red	0.64 - 0.67	30
Band 5 - Near Infrared (NIR)	0.85 - 0.88	30
Band 6 - SWIR 1	1.57 - 1.65	30
Band 7 - SWIR 2	2.11 - 2.29	30

Bands	Wavelength (μm)	Resolution (m)
Band 8 - Panchromatic	0.50 - 0.68	15
Band 9 - Cirrus	1.36 - 1.38	30
Band 10 - Thermal Infrared (TIRS) 1	10.60 - 11.19	100
Band 11 - Thermal Infrared (TIRS) 2	11.50 - 12.51	100

For the purpose of this project temperature data of 16 meteorological stations in Thessaly region were utilized. The prevailed atmospheric conditions during the meteorological measurements did not considerably affect the procedure. Useful characteristics of the used stations are located in Table A1 in Appendix A.

2.7 Land Use Land Cover data

Corine land cover (CLC) is a geographic land cover/land use database for a pan-European region (www.eea.europa.eu). It is produced by the European Environment Agency and provides consistent information on land cover across Europe using a nomenclature of 44 standard classes which are organized in 3 levels of detail (Stathopoulou and Cartalis, 2007) , as shown in Table 2.2.

Several operations have been done in the area of Greece and which use the CLC database. Some of them deal with UHII detection in combination with land use/land cover data (Stathopoulou et al., 2005; Stathopoulou and Cartalis, 2007; Stathopoulou and Cartalis, 2011), others with retrievals of turbulent heat fluxes and soil moisture content by remote sensing (Petropoulos and Carlson, 2011), detection and prediction of diachronic land cover changes (Perakis, 2011), land use classification using neural networks and remote sensing (Stathakis, 2003; Stathakis, 2009).

For the needs of this study, 6 main classes were created. 1) "Urban": Consisting of "Continuous urban fabric" and "Discontinuous urban fabric" inside city boundaries. 2) "Suburban": Consisting of "Green urban areas", "Discontinuous urban fabric" regions at city edge, two rural villages with less than 1000 citizens each and the semi-urban town of Giannouli, with 7885 citizens approximately (el.wikipedia.org). 3) "Rural" which stands for "Agricultural areas". The rural areas were chosen to have similar altitude to the urban area and not to be covered by continuous urban fabric. 4) "Industrial or commercial units" (Ind/ Comm). 5) "Airport". 6) "Water". Initially, 272 polygons were created, which during the study were merged or splitted, according to the needs of the comparisons. It should be noted that these classes reflect the backbone of the comparisons for the retrieval of UHI. Details about these classes can be found in Chapter 3. In addition, individual comparisons were performed and the results are discussed in Chapter 4.

Table 2.2: CLC database classes and an example of grouping land use classes (adapted from Stathopoulou and Cartalis, 2007)

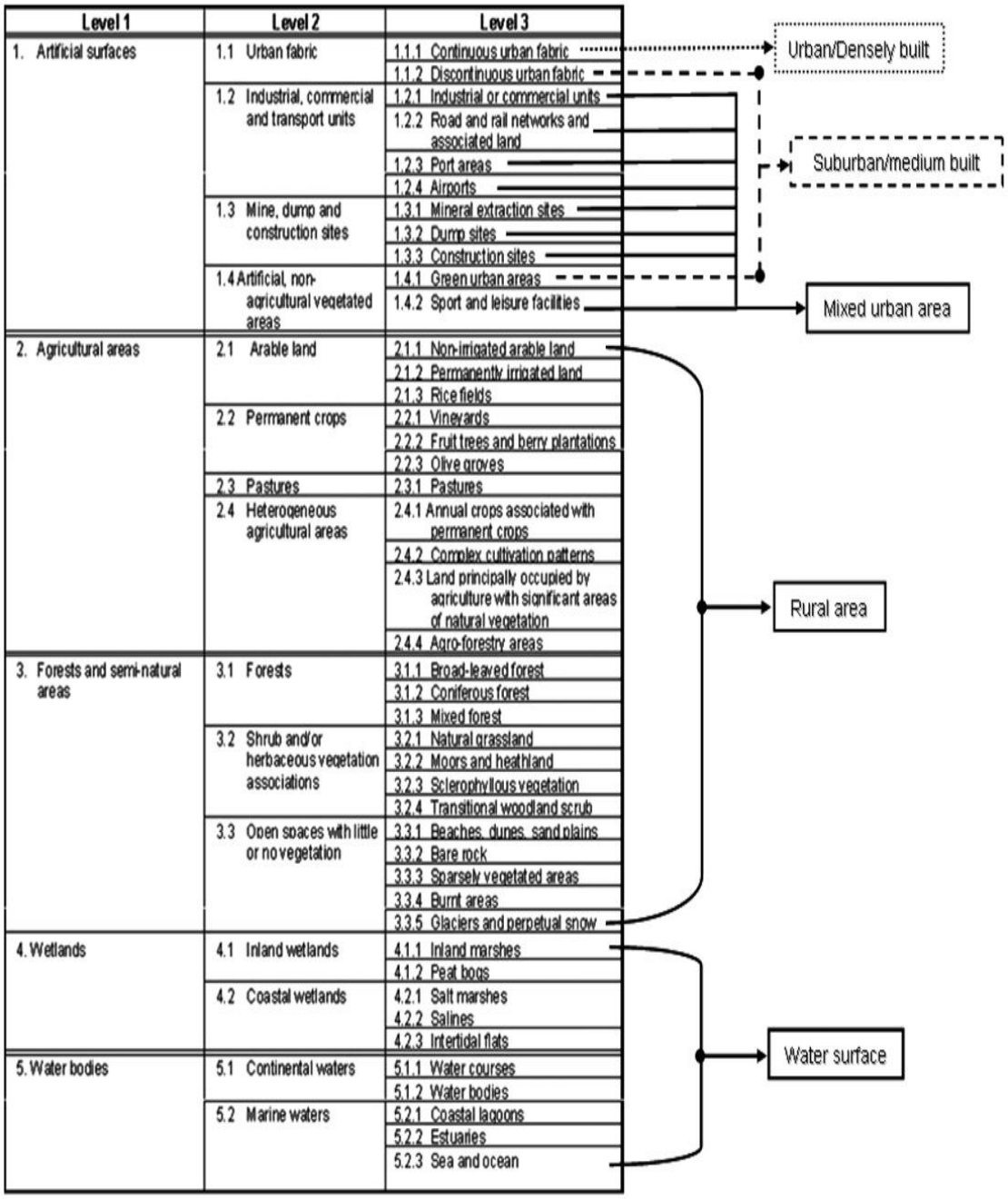

3 METHODOLOGY

3.1 Image Preprocessing

Landsat images were projected to the Greek Grid projection system (ellipsoid Geodetic Reference System 80, datum Greek Geodetic Reference System 1987 (GGRS ‘87)) and were georeferenced through Hellenic Cadastre and Mapping Agency base map using more than 20 ground control points for each pair of images. The points were chosen to be as discrete as possible, like highway intersections, evenly distributed across each image. ENVI 4.7 environment was used for the correction with nearest neighbor resampling before calibrating, converting to GGRS ’87 and exporting them to ArcMap 10.1, using the same projection system, for further analysis. The Root Mean Square (RMS) errors were less than 0.25 pixels (7.5 m) for each of the six pairs of images. In order to normalize the data, that is, to minimize the effects of bias arising from atmospheric conditions, solar illumination and view angles, atmospheric calibration is required. This would allow quantitative comparison between images taken at different times (Hoyos, 2014). In this project, after the images were clipped for practical and scientifical purposes, the conversion from digital number (DN) to radiance, reflectance and at-satellite brightness temperature followed the guideline found at the USGS website. Calibration parameters were directly accessed from the metadata file and all images were atmospherically corrected.

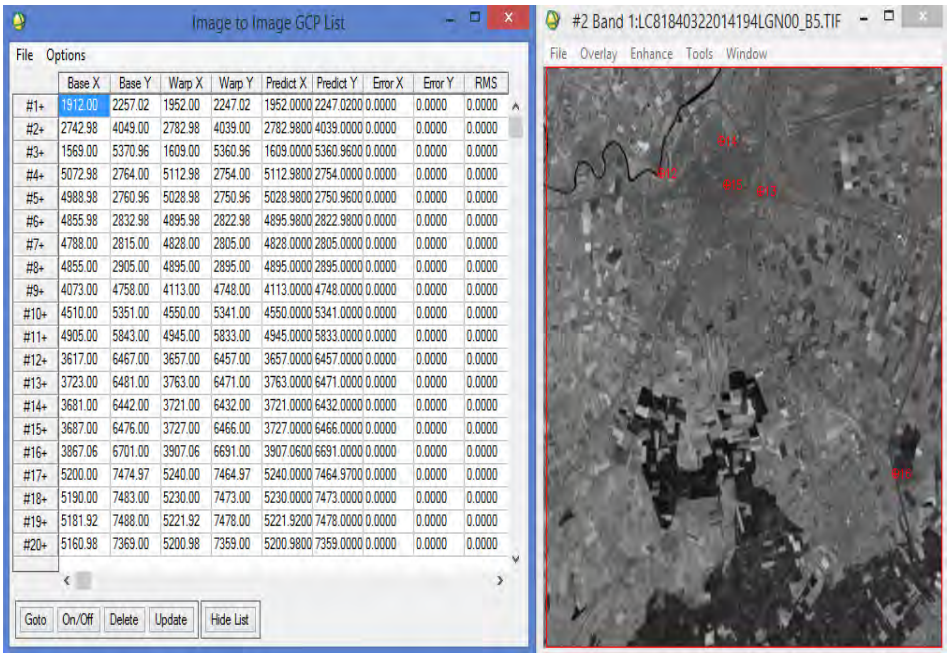

Figure 3.1: Example of wrapping 27/06/2014 with 13/07/2014 image, using 20 ground control points (GCP) in ENVI environment. Left part shows RMS and right part 5 GCP's in Larissa city, applying Band 5 scene of 13/07/2014 image.

3.2 Deriving At - Satellite Brightness Temperature

According to USGS website, standard Landsat 8 data products provided by the USGS Earth Resources Observation and Science (EROS) Center consist of quantized and calibrated scaled Digital Numbers (DN) representing multispectral image data acquired by both the Operational Land Imager (OLI**)** and Thermal Infrared Sensor (TIRS). The products are delivered in 16-bit unsigned integer format and can be rescaled to the Top Of Atmosphere (TOA) reflectance and/or radiance using radiometric rescaling coefficients provided in the product metadata file (MTL file), as briefly described below. The MTL file also contains the thermal constants needed to convert TIRS data (band 10 and 11) to the at-satellite brightness temperature.

TIRS band data were converted to TOA spectral radiance using the radiance rescaling factors provided in the metadata file:

$$L_\lambda = \mathrm{M}_L \times Q_{cal} + A_L \qquad (1)$$

where: L_λ = TOA spectral radiance (Watts/(m^2 × srad × μm))

M_L = Band-specific multiplicative rescaling factor from MTL file (RADIANCE_MULT_BAND_x, where x is the band number)

A_L = Band-specific additive rescaling factor from the metadata (RADIANCE_ADD_BAND_x, where x is the band number)

Q_{cal} = Quantized and calibrated standard product pixel values (DN)

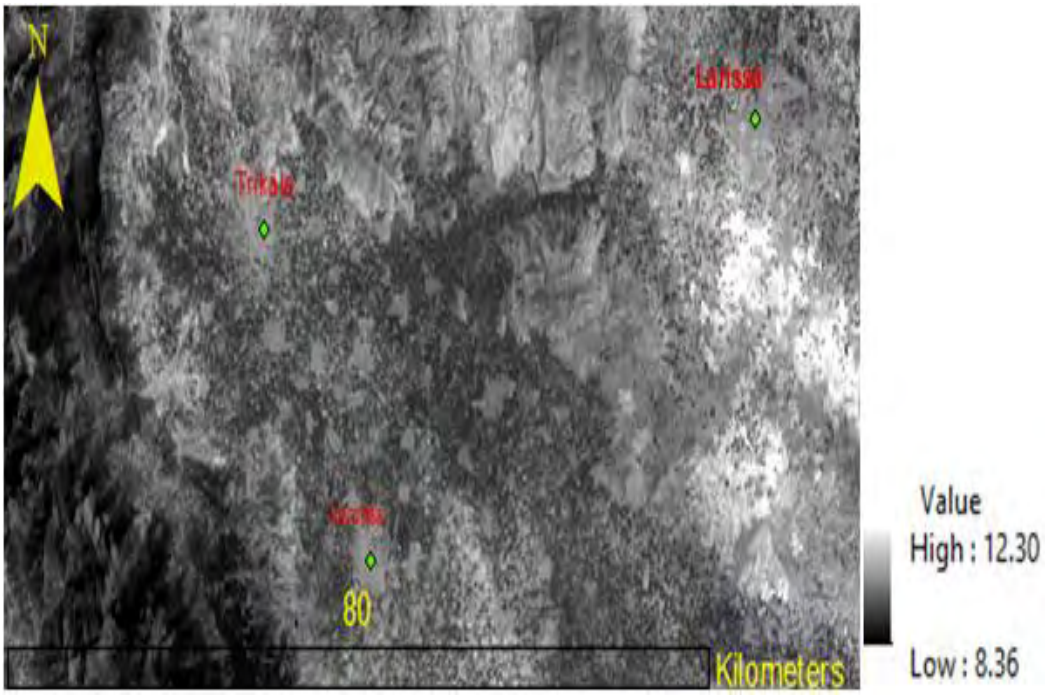

Figure 3.2: Band 10 converted to TOA spectral radiance scaled from 8.36 to 12.30 (Watts/(m^2 × srad × μm)) **)**

TIRS band data (Band 10 and 11) can be converted from spectral radiance to brightness temperature by using the thermal constants provided in the metadata file and the following equation:

$$T_B = \frac{K_2}{\ln(\frac{K_1}{L_\lambda}+1)} \quad (2)$$

where: T_B = At-satellite brightness temperature (Kelvin)
L_λ = TOA spectral radiance (Watts / (m^2 × srad × μm))
K_1 = Band-specific thermal conversion constant from the metadata file
K_2 = Band-specific thermal conversion constant from the metadata file (landsat.usgs.gov/Landsat8_Using_Product.php)

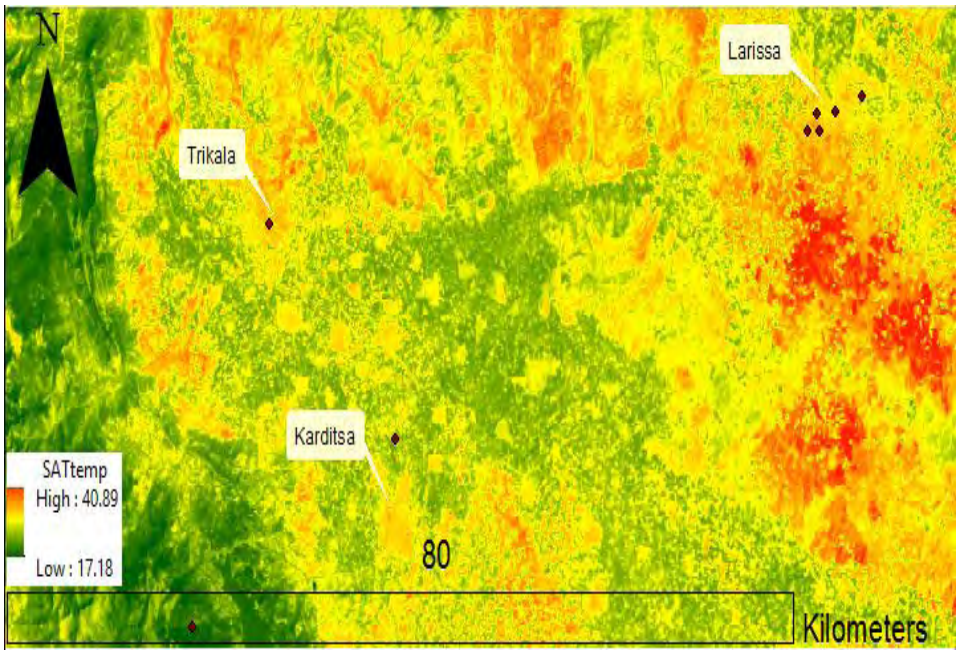

Figure 3.3: The mean At-Satellite Brightness Temperature (°C) of TIRS bands in 01/08/2015 image (103.3 × 44.7 km^2).

In Fig. 3.3 deep red coloured points depict 8 meteorological stations. From bottom-left to top-right: 1) Plastira Lake-National Observatory of Athens (N.O.A) station, 2) Karditsa (N.O.A) station, 3) Trikala (N.O.A) station, 4) Larissa (N.O.A) station, 5) Larissa-"sifnou" station, 6) Larissa-"6 dromoi" station, 7) Larissa-"ATA" station, 8) Larissa- Hellenic National Meteorological Service (HNMS) station.

3.3 Land Surface Emissivity Estimation

Land surface emissivity retrieval over agricultural regions is important for energy balance estimations, land cover assessment and other related environmental studies (Jiménez-Muñoz et al., 2006). The emissivity of land, unlike that of oceans, can differ significantly from unity and vary with vegetation, surface moisture, roughness, and viewing angles (Yu et al., 2014). In the case study that Yu et al., performed in 2014 in China, two major methods were proposed for LSE estimation before LST retrieval: classification-based emissivity method (CBEM) and NDVI-based emissivity method (NBEM). The CBEM obtains the LSE image from a classification image, in which an emissivity value for each class is assumed in advance. Although it is widely applied, this may not be very operative because we need a good knowledge of the study area and emissivity measurements on the surface representatives of different classes coincident with the satellites transiting time. An alternative, operative procedure is the NBEM. Because of its simplicity, this method has already been applied to various sensors with access to Visible Near InfraRed (VNIR) data **(**Yu et al., 2014**).** According to Sobrino et al. (2006), predicting surface emissivities from visible and near-infrared data provides

two main advantages to the NDVI method: i) sensors onboard satellites provide a higher spatial resolution for visible and near infrared than thermal infrared bands, so higher spatial resolution emissivity maps can be obtained, and ii) the NDVI method can be applied even to sensors with only one thermal band, provided that these sensors have red and near infrared bands, whereas another widespread method-Temperature Emissivity Separation (TES) method- needs at least four thermal bands (Yu et al., 2014).

Although Landsat8 TIRS consists of two thermal bands - Bands 10 and 11 - an important TIRS calibration notice from USGS, was taken into account, published on January 6, 2014: "Due to the larger calibration uncertainty associated with TIRS band 11, it is recommended that users refrain from relying on band 11 data in quantitative analysis of the TIRS data, such as the use of split window techniques for atmospheric correction and retrieval of surface temperature values. We suggest that Band 10 be used in conjunction with an atmospheric model to estimate surface brightness temperature. Our calibration team has found that with current processing these surface brightness temperatures are accurate to within ~ ±1 K for many 15 – 35° C targets, e.g., growing season vegetated targets " (http://landsat.usgs.gov/calibration_notices.php).

Eventually, the present study avoids applying split window techniques and makes use of the NDVI based method developed by Sobrino et al, (2004), according to which the final expression for LSE can be given by:

$$\varepsilon = 0.004 \times P_v + 0.986 \tag{3}$$

where ε is LSE, and P_v is the proportion of vegetation or Fractional Vegetation Cover (FVC), or Vegetation Fractional Cover (VFC) obtained according to (Carlson & Ripley, 1997):

$$P_v = \left[\frac{NDVI - NDVI_{\min}}{NDVI_{\max} - NDVI_{\min}} \right]^2 \tag{4}$$

For Landsat8 imagery, NDVI was calculated from red and near-infrared bands (band 4 and 5) from Operational Land Imager as following:

$$NDVI = \frac{\rho_5 - \rho_4}{\rho_5 + \rho_4} \tag{5}$$

where ρ_4 and ρ_5 are land surface reflectance after atmospheric correction. OLI band data (i.e.: band 4 and 5) have been converted to TOA planetary reflectance (ρ_4 and ρ_5) in two steps, using reflectance rescaling coefficients provided in the product MTL file. The following equation was used to convert DN values to TOA reflectance for OLI data as follows:

$$\rho_{\lambda'} = \mathrm{M}_\rho \times Q_{cal} + A_\rho \tag{6}$$

where:

$\rho_{\lambda'}$ = TOA planetary reflectance, without correction for solar angle.
M_ρ = Band-specific multiplicative rescaling factor from the metadata (REFLECTANCE_MULT_BAND_x)
A_ρ = Band-specific additive rescaling factor from the metadata (REFLECTANCE_ADD_BAND_x)
Q_{cal} = Quantized and calibrated standard product pixel values (DN)

TOA reflectance with a correction for the sun angle is then:

$$\rho_\lambda = \frac{\rho_{\lambda'}}{\cos(\theta_{SZ})} = \frac{\rho_{\lambda'}}{\sin(\theta_{SE})} \quad (7)$$

where:

ρ_λ = TOA planetary reflectance
θ_{SE} = Local sun elevation angle. The scene center sun elevation angle in degrees is provided in the metadata (SUN_ELEVATION).
θ_{SZ} = Local solar zenith angle; $\theta_{SZ} = 90° - \theta_{SE}$.
(landsat.usgs.gov/Landsat8_Using_Product.php)

The two maps in figures 3.4, 3.5 were produced by applying the above mentioned process in L8 image of 01/08/2015, at about 12:00 a.m, in ArcMap 10.1, environment. The regions in the images that are less vegetated, like structures, bare soil as well as those that are characterised by dense vegetation, like mountain tress can be detected. In the bottom left of the images, part of Plastira Lake is projected, and 3 out of 4 biggest cities in Thessaly. The patterns of these cities and Plastira Lake as well, are obvious, showing very low NDVI and VFC values, as expected. Visually, there seems to be a very high agreement, between the two maps, which is expected due to Eq. (4).

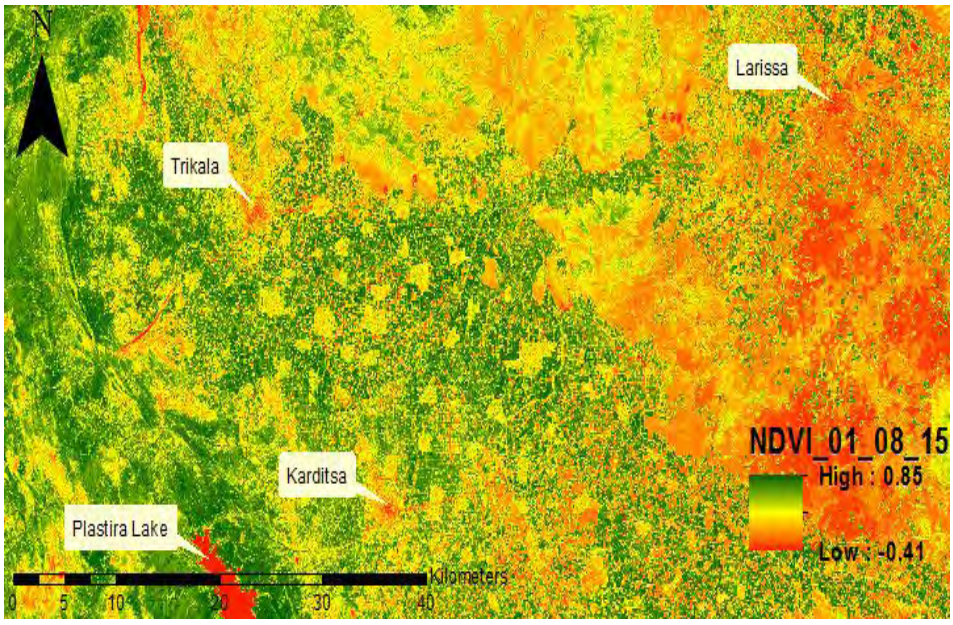

Figure 3.4: The spatial distribution map of NDVI in 01/08/2015 image (103.3 × 44.7 km^2).

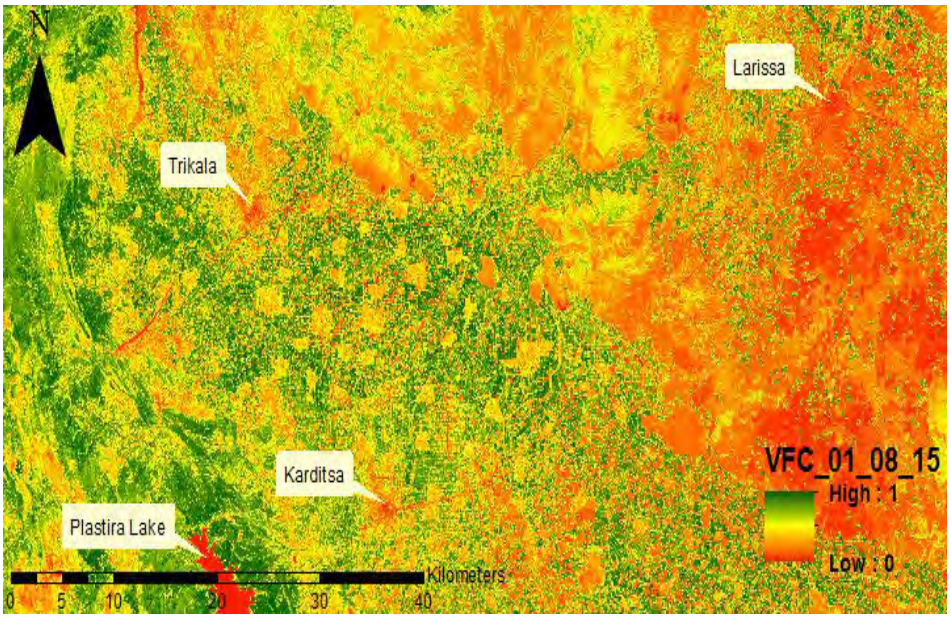

Figure 3.5: The spatial distribution map of VFC in 01/08/2015 image (103.3 × 44.7 km^2).

3.4 Land Surface Temperature Retrieval

Land surface temperature (LST) is a key parameter in the physics of the earth surface through the process of energy and water exchange with the atmosphere, which plays an important role in a wide variety of scientific studies, such as ecology, hydrology, and global change studies. Thermal infrared (TIR) remote sensing provides a unique method for obtaining LST information at the regional and global scales since most of the energy detected by the sensor in this spectral region is directly emitted by the land surface. Many efforts have been devoted to establish methods for retrieving the LST from remote sensing data, and significant progresses have been made over the past decade (Yu et al., 2014).

The derivation of LST from Landsat TM data mainly involves three steps: radiometric calibrations, atmospheric and surface emissivity corrections, and characterization of spatial variability (Liu et al., 2015). The digital number of geometrically corrected Landsat 8 bands 10 and 11 were first converted to spectral radiance using Equation (1), and then converted to at-sensor brightness temperature with Equation (2). Since brightness temperature derived from Eq. (2) is the temperature that a blackbody would obtain in order to produce the same radiance at the same wavelength (λ = 10.8 μm for band 10), additional correction for spectral emissivity is required to account for the non-uniform emissivity of the land surface (Stathopoulou - Cartalis, 2007). After deriving LSE images for the different Landsat scenes, LST could be retrieved and converted to degrees Celsius. The emissivity corrected LST was computed, using the following equation developed by Artis and Carnahan (1982):

$$LST = \frac{T_B}{1 + (\lambda \times T_B / \rho) \ln \varepsilon} \tag{8}$$

$$\rho = \frac{h \times c}{\sigma} \tag{9}$$

where λ is the wavelength of emitted radiance (λ = 10.8 μm for band 10), σ is the Boltzmann constant (1.38×10^{-23} J/K), *h* is the Planck's constant (6.626×10^{-34} Js), *c* is the velocity of light (2.998×108 m/s), ε = land surface emissivity.

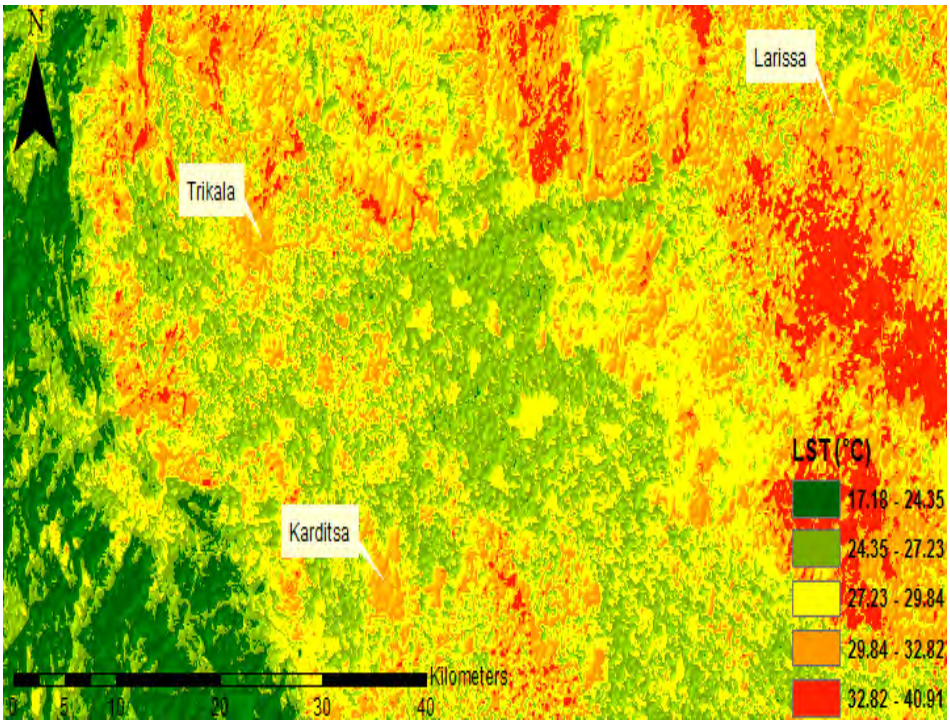

Figure 3.6: The spatial distribution of LST (°C) in 01/08/2015 image (103.3 × 44.7 km^2), the time that L8 passed over Thessaly.

3.5 Correlation – Validation procedure for LST

In order to investigate the validity of satellite retrieved temperature values (LST), a correlation - validation process has followed. 48 LST values from pixels in which the meteorological stations are located, identified in GIS environment (ArcMap, 10.1) and derived from six reprocessed Landsat images were correlated to maximum air temperature values measured from meteorological stations (Tmax), at the exact same dates (Figure 3.7).

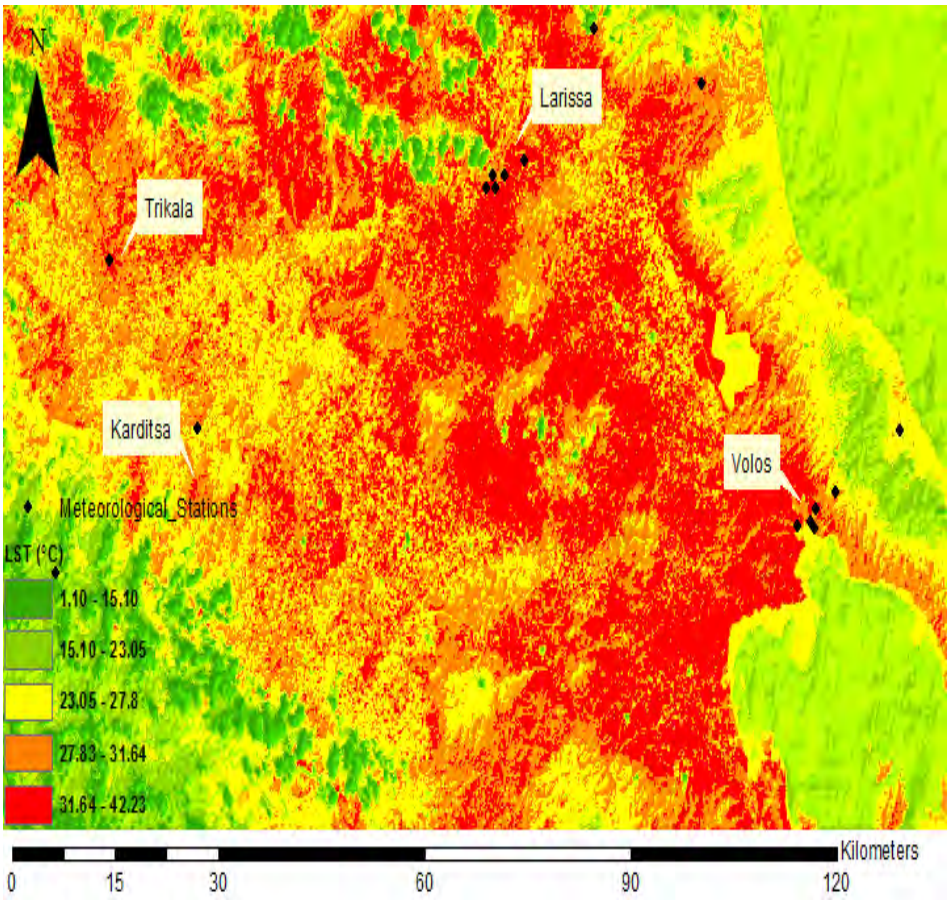

Figure 3.7: 17/08/2015 image, at 12:00 a.m. The 4 major cities of Thessaly and the 16 meteorological stations that were used in the correlation-validation process of LST.

The coordinates of each used pixel, in Fig. 3.8, are the same exactly with those that each meteorological station has. This can be accomplished by using Hellenic Cadastre and Mapping Agency, if and only if the projection system is the same, as in this case. Data from totally, 14 different stations were used (APPENDIX - Table A2) taking into account cloud cover over stations, possible frontal passages (leading to unusually high/low values) and technical malfunctions of stations. For instance, in 13/07/2014 image, five stations - Larissa city stations - were used in the correlation process because of clouds covering the other ones. The Pearson's correlation coefficient was found 0.86, with the following equation

$$y = 0.837x + 8.784 \quad (10)$$

showing the correlation between LST (x) and Tmax.(air) (y) - measured at meteorological stations.

The validity of LST values was examined by applying Eq. (10), with slope=0.837 and intercept=8.784 in a new L8 image, of 01/08/2015.

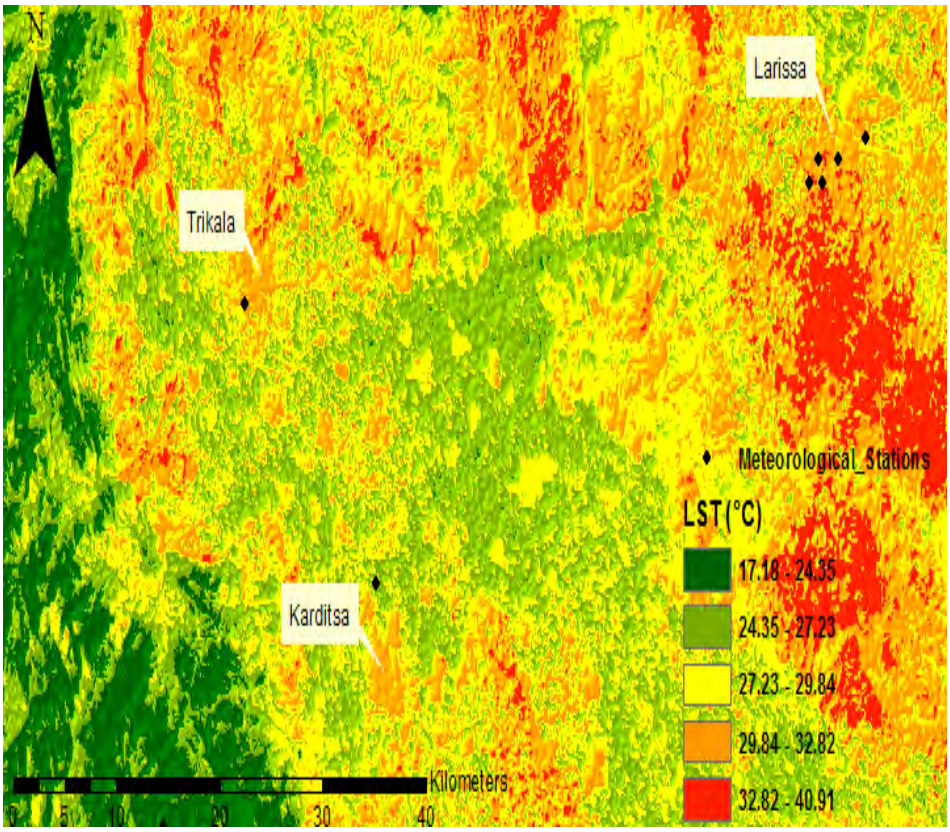

Figure 3.8: The 8 meteorological stations used in the validation procedure, and LST values at 12:00 a.m.

In the above map, of 01/08/2015, the distribution of meteorological stations that were used in the validation process is shown, in this part of Thessaly plain. In Fig. 3.8 deep red coloured points depict these 8 meteorological stations. From bottom-left to top-right: 1) Plastira Lake station, 2) Karditsa station, 3) Trikala station, 4) Larissa-(N.O.A) station, 5) Larissa-"sifnou" station, 6) Larissa-"6 dromoi" station, 7) Larissa-"ATA" station, 8) Larissa- (HNMS) station.

For the needs of the validity check, Eq. (10) was applied using 8 points in 01/08/2015 image and 8 measured Tmaximum values by meteorological stations. In this application, the input variable (x) was replaced by satellite retrieved, surface temperature values, (LST) and the output value (y) provided estimated maximum air temperature values (Testim.(air)). In this specific date, maximum air temperature values (Tmax. (air)) measured in 8 meteorological stations (Table 3.1) were available and they were compared to Testim.(air). The results showed a general average of ΔT = - 0.41 (°C), while average ΔT = - 0.22(°C) for Larissa stations, where ΔT stands for the

difference between Testim. and Tmax. The results (Table 3.1 and Fig. 3.10) show that LST values are enough valid, in order to be applied in every pixel of 01/08/2015 image, for the needs of the study.

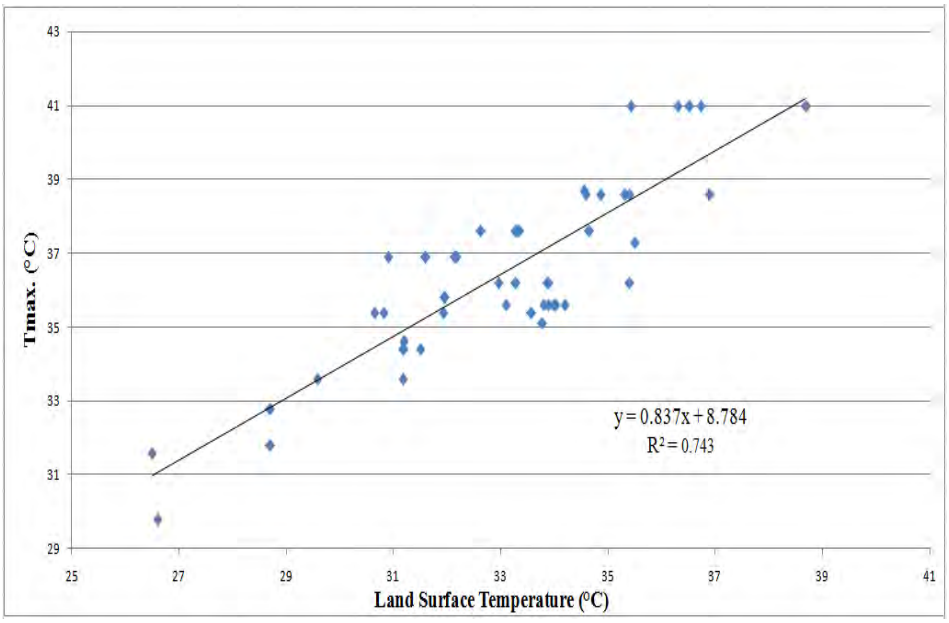

Figure 3.9: The correlation scatter plot between LST and Tmax, with coefficient of determination (R^2 = 0.743).

Table 3.1: Results of validation process for LST values, applying Eq.10. Elevation in m. and Temperatures in °C.

Stations	Elevation	LST	Tmax.(air)	Testim.(air)	Testim. - Tmax.
Larissa-"6 dromoi"	85	30.6	34.7	34.40	-0.30
Larissa-N.M.A	72	30.66	34.7	34.45	-0.25
Larissa-"sifnou"	82	30.38	34.7	34.21	-0.49
Larissa-"ATA"	81	30.52	34.7	34.33	-0.37
Larissa-N.O.A	82	31.34	34.7	35.02	0.32
Trikala-N.O.A	163	30.4	34.6	34.23	-0.37
Karditsa-N.O.A	91	30.3	34.3	34.15	-0.15
Plastira Lake	860	22.22	29.1	27.38	-1.72

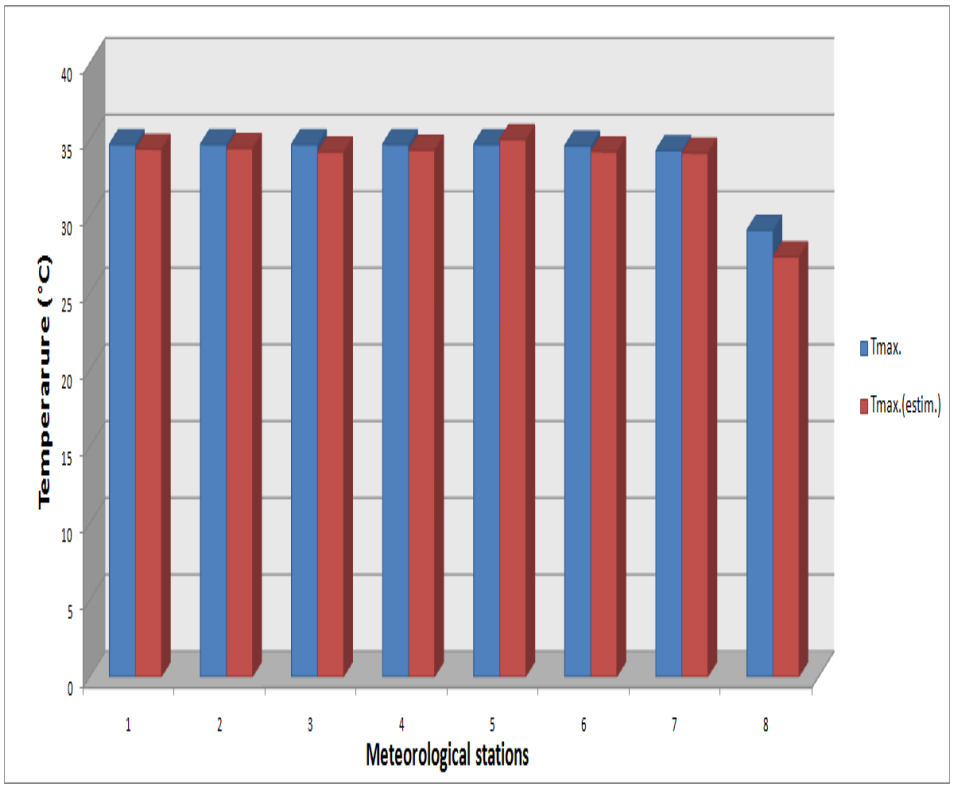

Figure 3.10: The difference between Tmax. and Tmax. estimated ranges from -1.72 to 0.32 °C, with average ΔT equal to -0.41 (°C).

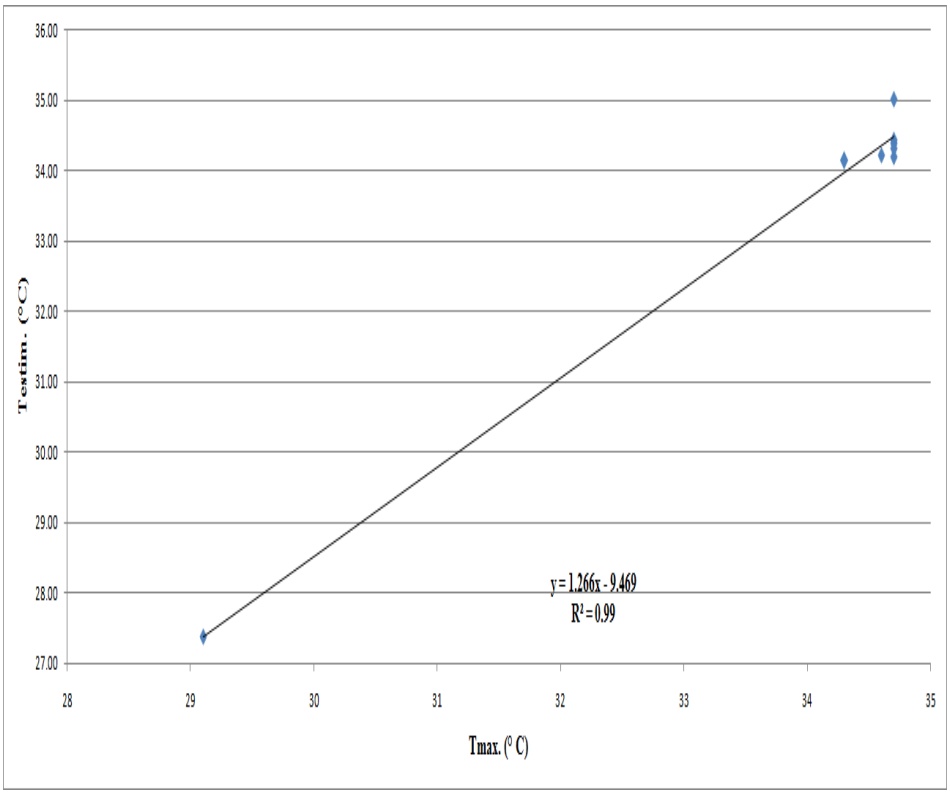

Figure 3.11: The correlation between Tmax. (air) and Tmax estimated (air) is very high, with R = 0.995.

3.6 Investigation of correlation between NDVI, VFC and LST

LSTs correspond closely with near surface temperatures and can therefore be considered a reliable indicator of the UHI. Vegetation abundance is also known to influence LSTs and UHI conditions through the process of evapotranspiration. Therefore, investigation into the relationship between NDVI and LST becomes informative and meaningful, especially concerning areas where the UHI phenomenon is more pronounced and where mitigation measures are needed (Farina, 2012). Given that vegetation abundance is known to reduce LSTs through the transfer of latent heat from the surface to atmosphere via evapotranspiration, NDVI can be used to investigate this relationship and thereby, provide insight into how this natural cooling mechanism of vegetation might be employed to help improve urban thermal environments. In general, areas with high NDVI are expected to have lower LSTs, however, this correlation may be influenced by soil moisture conditions and evapotranspiration of the surface (Yuan and Bauer, 2007; Su et al., 2010).

A correlation analysis between LST and NDVI, as long as LST and VFC, based on values of 66 points, in 01/08/2015 image, was conducted. The map was clipped in the extents of Larissa region and the points were selected to be representative of 6 land

cover types, based on the description of Chapter 2. The correlation coefficients between: LST-NDVI, LST-VFC, NDVI-VFC were found -0.809, -0.813, 0.999 respectively. The results of this analysis are depicted in Figures 3.7 and 3.8. It should be mentioned that class "Airport" was considered as part of the class "Ind/ Comm" and merged into this class. The "Rural" class was splitted into the two classes which constitute it and are dominant in the region of interest: "Non-Irrigated arable land" and "Permanently Irrigated land". Eventually, only for the needs of this specific correlation analysis, 6 different land cover types and 11 pixels per type were used, evenly distributed in Larissa region. The six classes were: "Urban", "Ind/ Comm", "Suburban", "Non-Irrigated arable land", "Permanently Irrigated land", "Water".

Inspired by CLC database: "Urban" was considered to be land that is covered by structures and transport network. Buildings, roads and artificially surfaced areas cover more than 80 % of the total surface. Non-linear areas of vegetation and bare soils are exceptional. "Ind/ Comm" refers to artificially surfaced areas (cement, asphalt, tar macadam or stabilized e.g. beaten earth) without vegetation occupying most of the area, which also contains building and/or vegetation. "Suburban" areas consist of "Green urban areas", "Discontinuous urban fabric" regions at city edge, two rural villages with less than 1000 citizens each and the semi-urban town of Giannouli, with 7885 citizens approximately, as mentioned in Chapter 2. "Green urban areas" are areas with vegetation within the urban fabric, including parks, cemeteries with vegetation, and mansions and their grounds. In "Discontinuous urban fabric" most of the land is covered by structures. Buildings, roads and artificially surfaced areas are associated with vegetated areas and bare soils, which occupy discontinuous but significant surfaces. It includes private housing estates, residential suburbs made of individual houses with privative gardens and/or small squares. Also, scattered blocks of residential flats, hamlets, small villages where numerous un-mineralized interstitial spaces: gardens, lawns can be distinguished. "Non-Irrigated arable land" includes cereals, legumes, fodder crops, root crops and fallow land. Includes flowers and tree (nurseries cultivation) and vegetables, whether open field or under plastic or glass (includes market gardening). Includes aromatic, medicinal and culinary plants. "Permanently Irrigated land" refers to crops irrigated permanently or periodically, using a permanent infrastructure (irrigation channels, drainage network). Most of these crops could not be cultivated without an artificial water supply. This specific class does not include sporadically irrigated land (www.eea.europa.eu).

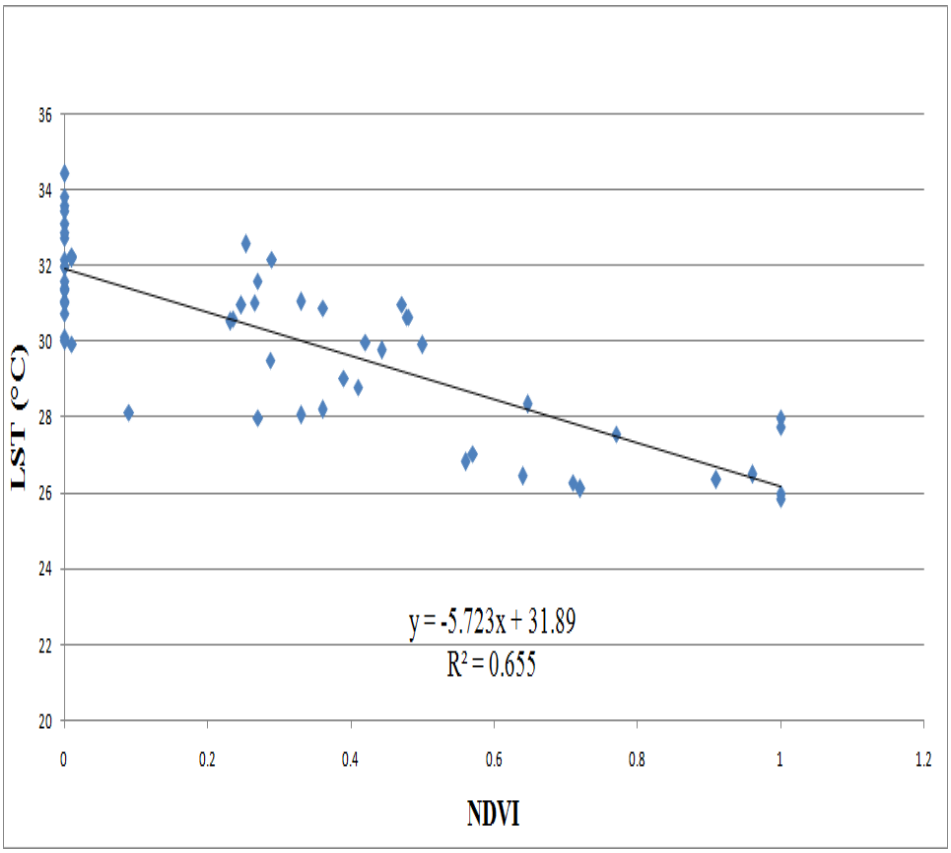

Figure 3.12: The scatter plot of correlation function between LST and NDVI, for 55 pixels, excluding "water" features.

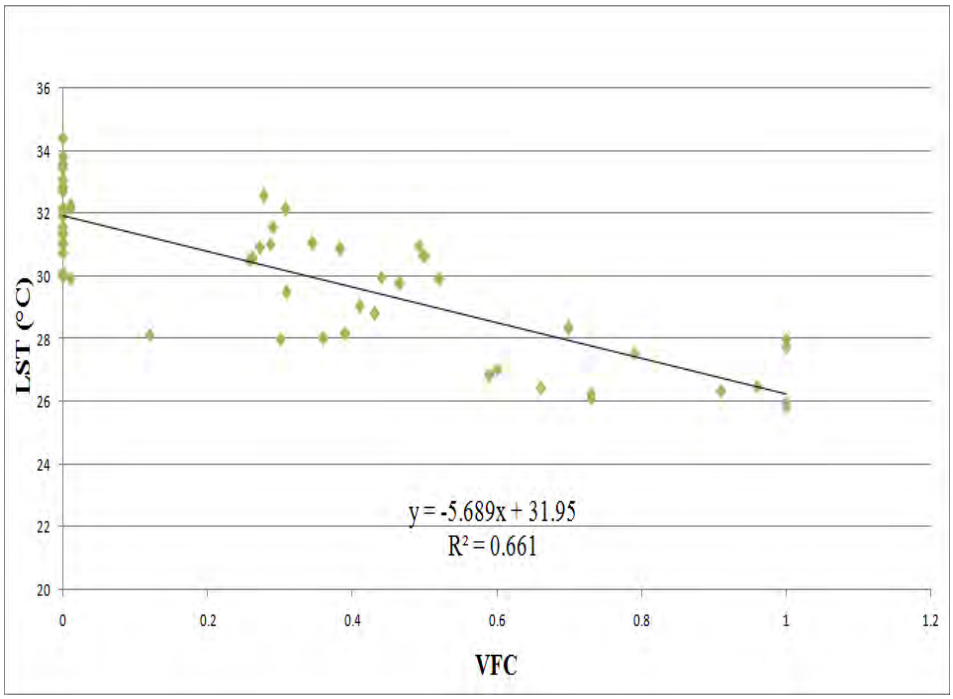

Figure 3.13: The scatter plot of correlation function between LST and VFC, for the same 55 points as in Figure 3.12.

3.7 Estimation of UHI Intensity

3.7.1 Polygon summary technique

The surface UHI intensity estimation was performed by combining the surface temperature data (in raster format) with the reproduced land cover data (in vector format), taking into account Corine 2000 data and possible changes in land cover. In particular, the land cover map (polygon layer) and the surface temperature image of the city (01/08/2015) were superimposed and minimum LST, mean LST with standard deviations (std) and the area were computed for each land cover class by using a polygon summary Geographical Information Systems (GIS) operation (Zonal statistics), (Stathopoulou - Cartalis, 2007). With the Zonal Statistics tool, a statistic is calculated for each zone defined by a zone dataset, based on values from another dataset (a value raster). A single output value is computed for every zone in the input zone dataset. A zone is all the cells in a raster that have the same value, whether or not they are contiguous. The input zone layer defines the shape, values, and locations of the zones and the input value raster contains the input values used in calculating the output statistic for each zone (http://resources.arcgis.com). An example of zonal statistics tool is located in Figure A1 in Appendix A.

In this way, the intensity of the surface UHI (ΔT) is estimated from the surface temperature differences between the Urban region (U), Commercial/Industrial area (C/I), Suburban area (S), (based on Corine 2000 and at site optical observations) and the

surrounding Rural area (R) of the city. UHII can be calculated by subtracting the mean LST value of one land cover class from the mean LST value of another one. For polygon summary operation and supervised classification, the number of polygons that was created, after a detailed procedure, was initially 272, as following. Urban area: 75, water: 45, suburban: 15, rural: 100, urban vegetation: 11, comm/ind: 25, airport: 1. After the conduction of some conclusions which are discussed in Chapter 4, by comparing mean LST values of Urban with suburban areas, it was decided to merge suburban with urban vegetation.

Mean surface temperatures by 6 land cover classes are given in Table 3.2, whereas surface UHI intensities of Larissa city are presented in Table 3.3, where ΔT denotes the mean LST difference or in other words UHII, in between U–R, C/I–R and S–R areas. Generally, in similar researches the main difference which is examined and that shows the UHII (ΔT) is that between U and R. The other differences are investigated for the conduction of further conclusions. In Chapter 4, these results are discussed.

Table 3.2: Mean values of LST, in °C, with std, and area of the used polygons per land cover type.

Land cover	Mean LST	Std	Area (Km^2)
Urban	31.52	1.37	17.71
Rural	29.73	2.51	86.67
Comm/ Ind	31.12	1.98	11.89
Suburban/medium built/urban veg.	29.83	2.26	5.41
Airport	29.95	1.38	9.29
Water	28.42	1.79	0.3

Table 3.3: Estimated UHII (ΔT), in °C, based on 6 main classes, using the polygon summary approach in GIS.

City	ΔT_{U-R}	ΔT_{S-R}	$\Delta T_{C/I-R}$
Larissa	1.79	0.1	1.39

3.7.2 Classification Approach

Apart from the above procedure, unsupervised and supervised classification methods were applied, for the estimation of UHII, exploring 3 different cases (7, 6, 4 classes) in both methods. In GIS, Iso Cluster unsupervised classification was performed as well as Maximum Likelihood (M-L), which is a supervised classification technique (by Spatial Analyst toolbox in ArcMap).

M-L Classification was performed, using the specific polygons that were used in polygon summary technique, as input signature file. This tool considers both the variances and covariance of the class signatures when assigning each cell to one of the classes represented in the signature file. With the assumption that the distribution of a class sample is normal, a class can be characterized by the mean vector and the covariance matrix. Given these two characteristics for each cell value, the statistical probability is computed for each class to determine the membership of the cells to the

class. When the default “EQUAL - A priori probability weighting” option is specified, each cell is assigned to the class to which it has the highest probability of being a member. For post classification procedure, in the classified map, the Majority Filter tool was used to generalize the edges of zones in the map (raster). The edges were smoothed to varying degrees either by expanding and shrinking boundaries or by growing or shrinking zones based on the values within the neighbourhood of individual locations (http://resources.arcgis.com). As in polygon summary technique, in M-L and Iso Cluster approach, the needed statistics were calculated by means of zonal statistic tool in GIS environment.

ML - classification was initially performed with 7 classes: Urban, Water, Suburban, Urban Vegetation (UV), Comm/Ind (C/I), Non-irrigated (N/I), Permanently Irrigated (P/I). This distinction for the classes was selected so as to identify possible temperature differences between non-irrigated and permanently irrigated land. Additionally, class “Airport” was chosen to be merged with C/I, since they belong in the same Level 2 class: “Industrial, commercial and transport units” according to CLC database. The results of UHII are discussed in the following chapter. Additionally, the ΔUHIIs were estimated, dealing with the range of UHII. For example, $\Delta UHII_{U\text{-}P/I}$ refers to the range which consists of two differences. The difference between mean LST of Urban and mean LST of P/I is the lower bound, while the difference between mean LST of Urban and minimum LST of P/I is the upper. $\Delta UHII_{U\text{-}P/I}$ was found to extend from 1.62 to 6.66 (°C), and $\Delta UHII_{U\text{-}N/I}$ from 0.68 to 6.81 (°C), concerning the differences between urban and rural composites.

Estimation of UHII and ΔUHII by means of ML - classification with 6 classes including Urban, Water, Suburban, Rural, C/I, UV was also performed and the results are shown in Tables 3.4, 3.5 and 3.6.

Table 3.4: Mean values of LST, in °C, with std, and minimum LSTs, applying ML classification with 6 classes.

Land cover	Min. LST	Mean LST	Std
Urban	24.41	30.93	2.04
Rural	24.18	29.83	2.44
Comm/Ind	24.42	30.62	2.49
Suburban	24.43	29.72	2.44
Urban Vegetation	24.24	29.42	2.22
Water	24.61	29.47	2.12

Table 3.5: Results of applying supervised classification with maximum likelihood approach, for estimation of UHII (ΔT), in 6 classes.

City	$\Delta T_{U\text{-}R}$ (°C)	$\Delta T_{S\text{-}R}$ (°C)	$\Delta T_{C/I\text{-}R}$ (°C)
Larissa	1.1	-0.1	0.79

Table 3.6: Results of applying supervised classification with maximum likelihood approach, for estimation of ΔUHII in °C, in 6 classes.

City	$\Delta UHII_{U-R}$	$\Delta UHII_{S-R}$	$\Delta UHII_{C/I-R}$
Larissa	1.1 - 6.75	-0.1 – 5.54	0.79 – 6.44

Afterwards, ML-classification with 4 classes including Urban (merged with comm/ind and airport), Water, Suburban, Rural, was performed for the estimation of UHII and ΔUHII. The ΔUHIIs were found as following: $\Delta UHII_{U-R}$ = 1.25 - 6.76 °C, $\Delta UHII_{S-R}$= 0.97 - 6.48 °C.

In the following Fig. 3.14, 3.15 (M-L with 7 classes) the different land cover types are identified quite sufficiently and UHII is identified optically, with urban area presenting the highest mean LST of 30.97 °C while the lowest mean LST of 29.35 °C appears in permanent irrigated land. The visual pattern of ML classification with 6 classes is not presented here, but only the numerical results, as described above.

Table 3.7: Mean values of LST, in °C, with std, and minimum LSTs, applying ML classification with 4 classes.

Land cover	Min. LST	Mean LST	Std
Urban/comm/ind	24.33	30.94	2.21
Rural	24.18	29.69	2.37
Suburban	24.33	30.66	2.26
Water	24.37	29.54	2.12

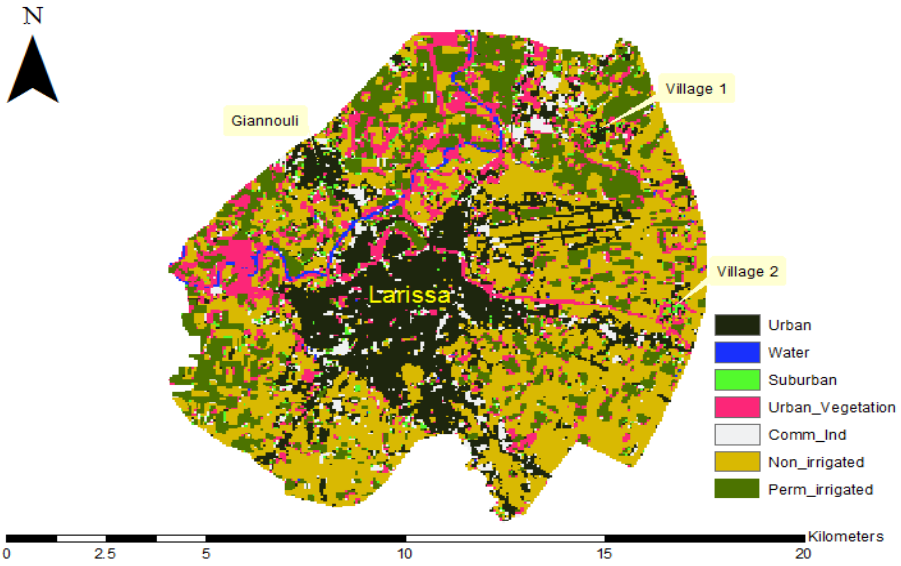

Figure 3.14: ML classification with 7 classes, using the majority filter tool, for post classification process.

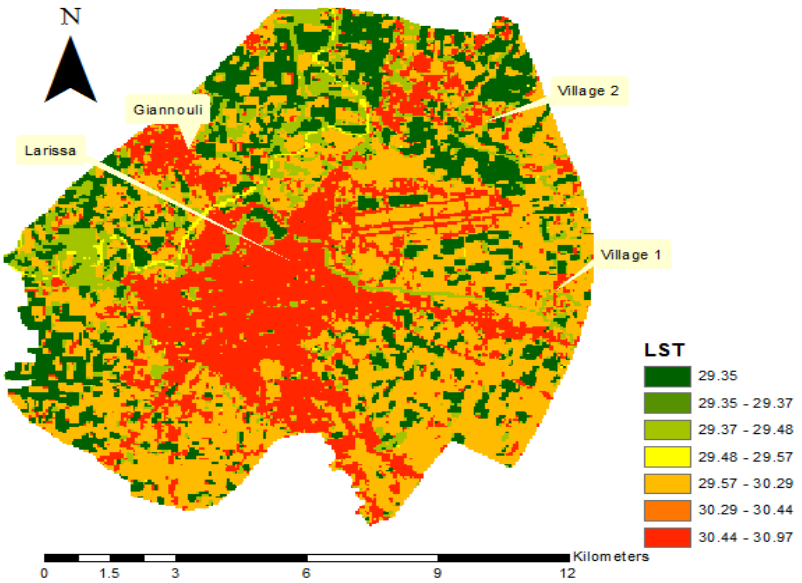

Figure 3.15: Classification of mean LST, by means of ML with 7 classes, using the majority filter tool, for post classification process.

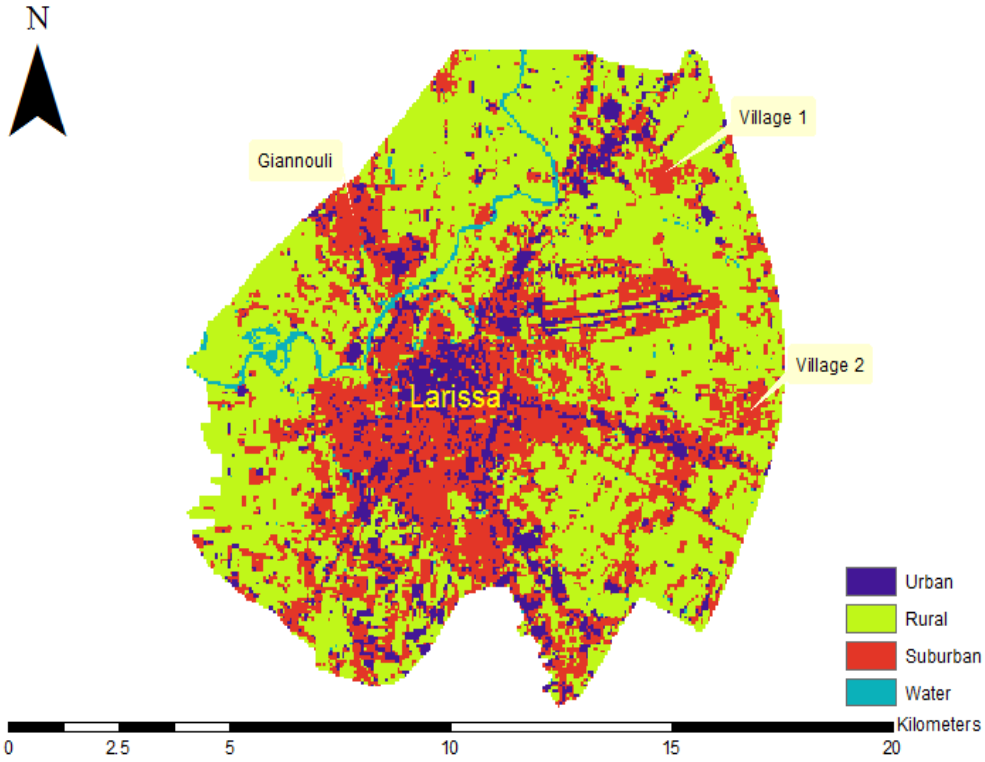

Figure 3.16: ML classification with 4 classes, using the majority filter tool, for post classification process.

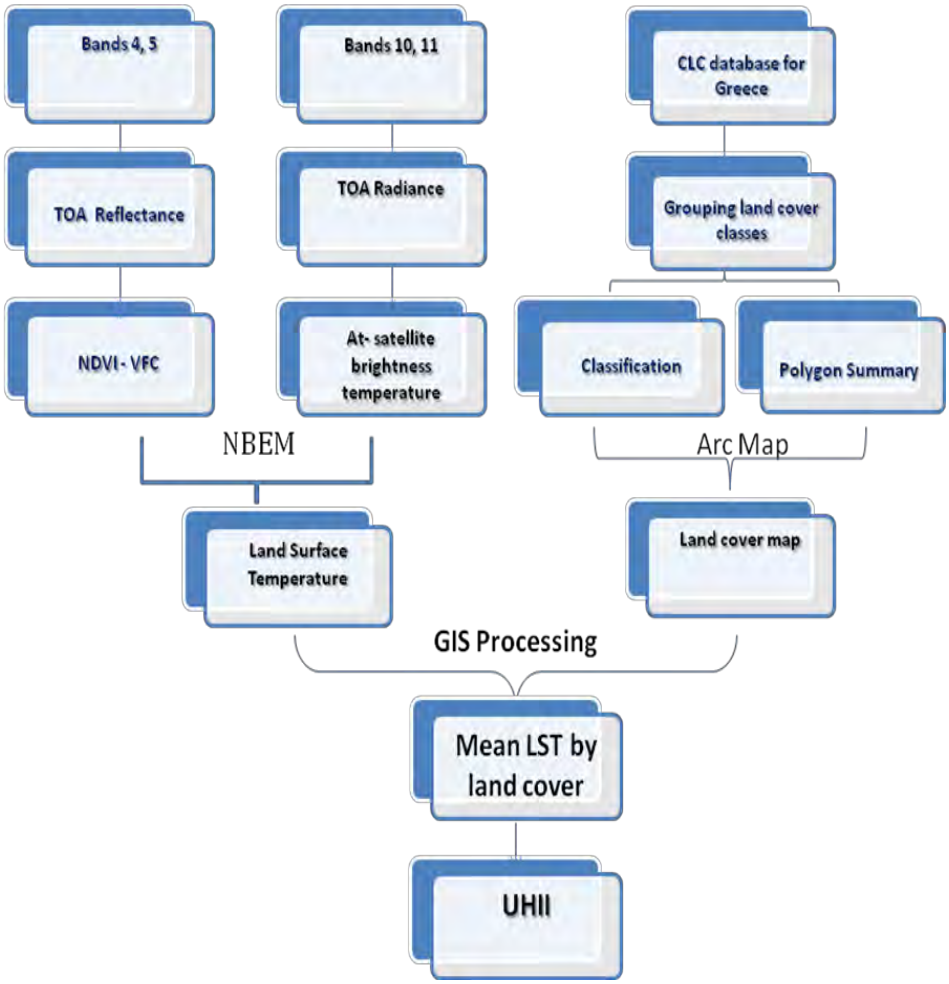

Figure 3.17: Flowchart of the methods leading to the estimation of the UHI intensity from satellite and Corine data.

4 RESULTS-DISCUSSION

4.1 Correlation analysis results for LST, NDVI and VFC

As it was mentioned above, the results from scatter plots 3.7, 3.8 indicate a significantly negative correlation between LST and NDVI for the study area. VFC shows a slightly stronger negative correlation with LST than NDVI, but equal increase in VFC and NDVI does not seem to cause the exact same decrease in LST. NDVI presents steeper slope in the correlation function and an increase of 0.1 in this index causes a decrease of approximately 0.572 °C in LST. An increase of 10% in VFC causes a decrease of approximately 0.568 °C.

Among the points that were used for the correlation analysis, the pixels with the highest LST values were located in urban and industrial/commercial areas, where vegetation presence is sparse, while the points that revealed the lower LST values were those of rural area, and especially those that belonged to permanently irrigated land. It must be emphasized that, in the region the lowest LST values were detected at water surface (Pineios river) but they, in pararrel, showed the lowest NDVI value, close to zero and even negative. This physiological attribute of "water pixels", resulted in executing two kinds of correlation analysis.

One, with including "water" and another, in which it is excluded. It is worth mentioned that, the water pixels spotted in this image showed a range from 26 to 28 °C LST and NDVI from 0 to 0.02. Including those points in the correlation analysis, the Pearson's coefficient (R) was found equal to -0.38 for LST vs. NDVI, while excluding water the R was, respectively, equal to -0.809. As for LST vs. VFC correlation analysis, excluding the water pixels R is equal to -0.813, while including it R was found -0.39.

These results may also suggest that for urban areas, LST can be estimated, through a statistical analysis, quite sufficiently, by knowing NDVI values and vice-versa. A possible thought may be that for areas which include water surfaces, the combined use of other indices, i.e.: Normalized Difference Water Index (NDWI) may be preferable. Since it is slightly easier to be retrieved, compared to VFC, it is more applicable to be under constant investigation, by means of satellites and ground research.

According to a research study of Sun & Kafatos (2007) in North America, the correlations between LST and Normalized Difference Vegetation Index (NDVI) depend on the season-of-year and time-of-day. In addition, they found out that for winter, the correlation between NDVI and LST is positive, while there is a strong negative correlation between LST and NDVI only during the warm seasons. Temperature-related drought indices may only be used in the warm seasons from May to October, and should be used with caution during cold seasons in North America. They also proved that the cooling effect of vegetation on LST is stronger during daytime than nighttime.

The visual results of the relation between NDVI, VFC and LST are revealed in Fig. 4.1, 4.2, 4.3 in which there seems to be an inverse relationship between LST and NDVI. Similarly, almost the same relation is illustrated between LST and VFC. Southern areas of the city, with the lowest values of vegetation cover, present to be more vulnerable to drought events. In connection with that, and according to Orhan et al., 2014; a drought index, which describes the temporal and spatial variations of crop water use status, can be suitable for drought monitoring. As climatic data, such as precipitation and air temperature, collected by weather stations have poor spatial resolution, satellite remotely sensed data offer considerable advantages and should be an integral part of monitoring drought, especially for detecting the temporal and spatial evolution of drought. NDVI not only maps the presence of vegetation on a pixel basis, but also provides measures of the amount or condition of vegetation within a pixel. LST is a good indicator of the energy balance at the Earth's surface because it is one of the key parameters in the physics of land-surface processes on regional and global scales.

Eventually, in Larissa region a further research can be done so as to examine if and how the correlations between LST and NDVI depend on the season-of-year and time-of-day. Additionally, if the cooling effect of vegetation on LST is stronger during daytime than nighttime.

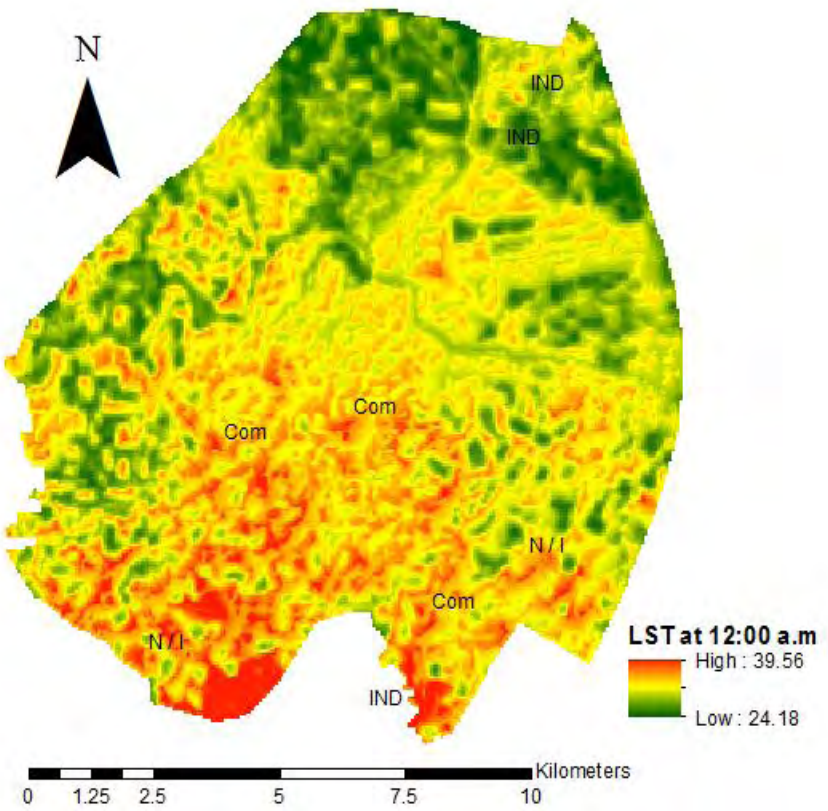

Figure 4.1. The spatial distribution of LST (°C) in 01/08/2015 image of Larissa region.

The visual inspection of LST distribution image, in Fig. 4.1, in combination with Fig. 4.2, 4.3 revealed ‘‘hot spots’’ of the region in the urban as well in the rural area. Some indicative “hot spots” are southern ind/com area and one in the northern area. Two commercial areas are depicted in southern urban area, about 1 km. distance from city center, and a non-irrigated part of land in southern region. The fore mentioned southern part of Larissa region, is more than easily detected, in deep red color, as well as the permanently irrigated lands, mainly located in the northern rural area, which present the lowest temperature values.

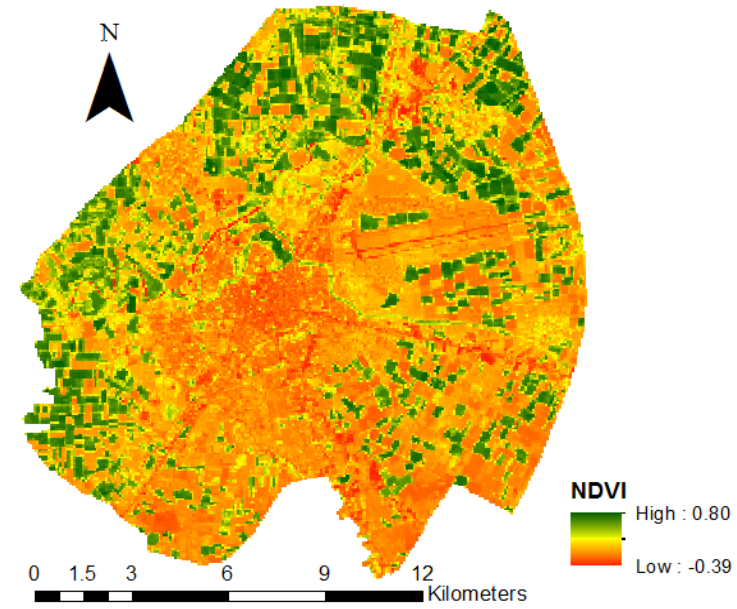

Figure 4.2. NDVI spatial distribution in 01/08/2015 image of Larissa region, at the time that L8 passes over Thessaly.

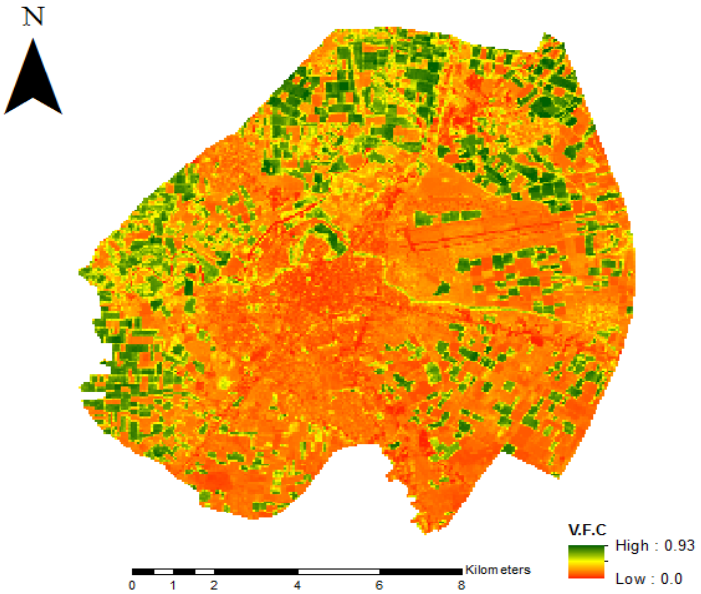

Figure 4.3. The spatial distribution of VFC (%) in 01/08/2015 image of Larissa region, at about 12:00 a.m.

4.2 UHII results

In the beginning of Larissa UHII examination, 11 classes were created based on land cover polygons. These classes are presented in Figure A4 in Appendix A. During the study they were merged or splitted, according to the needs of the comparisons. It must be noticed that, the comparisons of mean LST values, were made on Saturday, 01/08/2015 image, about 12:00 a.m, which is the overpass time of L8. It was found that a few bare soil fields covering an area of totally 8 km^2, in the southern part showed 33 °C mean temperature. This can be attributed to the fact that outdoor areas with bare dry soil are characterized by a low thermal inertia, which means that these regions exhibit large changes in their surface temperature from day to night, thus quickly heated during the day and also are cooled rapidly by overnight (Cracknell and Xue, 1995).

Permanently irrigated lands, mostly located in the northern part of Larissa region, and of 62 km^2 total area, revealed a mean temperature of about 29 °C. These lands are mostly crops irrigated permanently or periodically, using a permanent infrastructure (irrigation channels, drainage network). Arable area of non-permanently irrigated land, 26 km^2, mainly identified in the southern part, consisted primarily of cereals, fodder crops, root crops and fallow land in agreement with CLC. This very warm region showed a mean temperature of about 31 °C.

Regarding urban area and city parks (part of "urban vegetation"). The city center, central bus and train station were found warm enough, with a mean LST of approximately 31.8 °C and areas of military use inside the city around 34 °C. The main park in the city (Alkazar), located in the north-west part at about 1 km distance from the center, revealed a mean temperature of approximately 30.6 °C, meaning that it was about 1 °C cooler than the mean temperature of urban area. The other 3 urban parks, located southern, at 1-1.5 km. distance from city center, showed a mean temperature of approximately 31 °C, due to the fact that they present significantly less vegetation cover and density, compared to Alkazar park.

Acording to Ackerman, there are a number of factors that contribute to the relative warmth of cities: During the day in rural areas, the solar energy absorbed near the ground evaporates water from the vegetation and soil. Thus, while there is a net solar energy gain, this is compensated to some degree by evaporative cooling. In cities, where there is less vegetation, the buildings, streets and sidewalks absorb the majority of solar energy input. Additionally, since the cities have less water, runoff is greater in the cities because the pavements are largely nonporous (except by the pot holes). Thus, evaporative cooling is less which contributes to the higher air temperatures. Waste heat from city buildings, cars and trains is another factor contributing to the warm cities. Heat generated by these objects eventually makes its way into the atmosphere. This heat contribution can be as much as one-third of that received from solar energy. The thermal properties of buildings add heat to the air by conduction. Tar, asphalt, brick and concrete are better conductors of heat than the vegetation of the rural area. The canyon structure that tall buildings create enhances the warming. During the day, solar energy is trapped by multiple reflections off the buildings while the infrared heat losses are reduced by absorption (http://cimss.ssec.wisc.edu).

Concerning industrial areas, the northern industrial area shows up to 33.5 °C, while the southern one depicts 34 °C. The high surface temperatures observed at these industrial zones can be attributed to the local structure development comprising of low-

rise buildings along wide paved streets and extensive unshaded open spaces consisting of nonbuild areas and bare ground (Stathopoulou & Cartalis, 2007). Regarding suburban regions, it must be reminded that it consists of the 3 suburban towns of medium built, lower density suburbs in the city-edge, and urban vegetation. The "unified" region was found to obtain a mean LST of 29.83 °C, probably due to the lower values of mean LST that the 3 towns present, which were about 29 °C. Individually, urban vegetation was found to have approximately 30 °C, which is 1.5 °C cooler than the mean LST of urban area. City – edge areas presented mean LST of 30.4 °C.

The airport class was found 1.6 °C cooler than urban area and 0.1, 0.2 °C warmer than suburban and rural areas respectively. This finding is probably due to presence of very low vegetation cover inside the airport.

Generally, results of the estimated daytime UHI intensities for the city of Larissa on the 1st of August, 2015 show that central urban areas are 1.79 °C warmer than rural areas, whereas suburban areas are about 0.1 °C warmer than rural areas. Comm/Ind areas were found 0.4 °C cooler than urban ones and airport 1.6 °C cooler than urban.

As for ΔUHII, in this study it was found that UHII concerning urban and rural areas ranges from 1.79 to 7.39 °C, while for suburban and rural, ranges from 0.1 to 5.7 °C.

Table 4.1: Necessary measures in 01/08/2015 map in order to estimate UHII and ΔUHII, with polygon summary method.

Land cover	Area (Km^2)	Min. LST	Mean LST	Std
Urban	17.71	25.61	31.52	1.37
Rural	86.67	24.13	29.73	2.51
Comm/ Ind	11.89	24.25	31.12	2.21
Suburban/medium built	5.41	25.00	29.83	2.26

Applying unsupervised isocluster classification, the visual results showed that applying 7 classes, compared to 6 and 4 classes, the UHI is more intense numerically, but applying 6 classes, UHI is more obvious, visually. The optical results can be seen in Figures 4.4, 4.5, 4.6. Since in Iso Cluster Unsupervised Classification training samples were not produced from known locations of specific classes, it may be considered not so efficient for calculating exact values of UHII. Nevertheless, a more profound experiment in different number of thresholds, standard deviations, maximum distance errors and class pixel characteristic values in Iso Cluster could have provided better visual results.

As it is mentioned above, in ML classification with 7 classes approach, the ΔUHIIs stand for the extent of UHII, from minimum to maximum and were found as following: $\Delta UHII_{U\text{-}P/I}$ = 1.62 - 6.66 (°C), $\Delta UHII_{U\text{-}N/I}$ = 0.68 - 6.81 (°C), concerning the differences between urban and rural composites. These results were derived from the following Table 4.2.

Table 4.2: Mean values of LST, in °C, with std, and minimum LSTs, applying ML classification with 7 classes.

Land cover	Min. LST	Mean LST	Std
Urban	24.41	30.97	1.89
Perm. Irrigated	24.31	29.35	2.30
Non Irrigated	24.18	30.29	2.51
Comm/Ind	24.50	30.44	2.34
Suburban	24.66	29.57	2.29
Urban Vegetation	24.25	29.37	2.23
Water	24.61	29.48	2.11

The ΔUHIIs in ML-classification with 6 classes including Urban, Water, Suburban, Rural, Comm/Ind, and UV show greater similarity with polygon summary approach, concerning both ΔT_{U-R} and $\Delta T_{C/I-R}$. Despite the fact that they do not consist of the exact same classes, probably the same number of classes combined with the efficiency of the methods led to this result. ML-classification with 4 classes including Urban (merged with comm/ind and airport), Water, Suburban, Rural, was performed for the estimation of UHII and ΔUHII. The $\Delta UHII_{U-R}$ for 4 classes was found to range from 1.25 to 6.76 °C, and $\Delta UHII_{S-R}$ from 0.97 to 6.48 °C.

It must be mentioned that, ML approach is applied more than every other classification method providing in many cases an efficient result. As it is mentioned above, is based on the premise that values of the sample areas and categories follow the normal distribution, which is not always verified in practice (Stathakis, 2003).

Table 4.3: Comparison between two different approaches for ΔUHII in °C. The methods that show the greatest similarity are shown.

Method	$\Delta UHII_{U-R}$	$\Delta UHII_{S-R}$	$\Delta UHII_{C/I-R}$
ML-6classes	1.1 to 6.75	-0.1 to 5.54	0.79 to 6.44
zonal summary	1.79 to 7.39	0.1 to 5.7	1.39 to 6.99

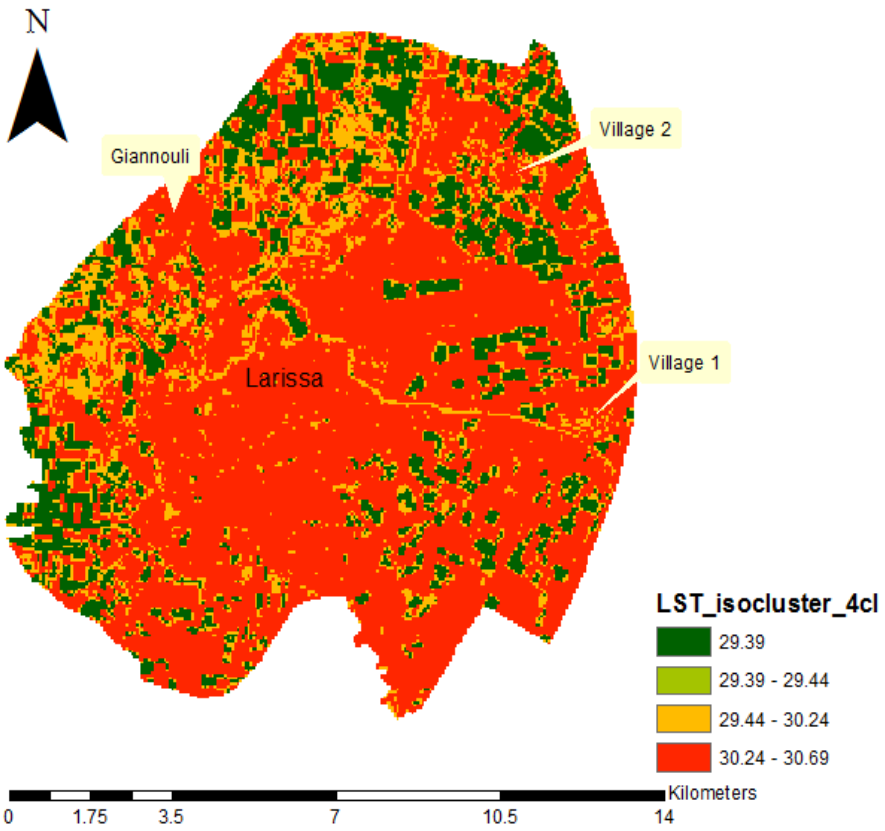

Figure 4.4: Mean LST values in Larissa region, at 01/08/2015.

In the above figure the isocluster unsupervised classification with 4 classes was applied. Rural areas show lower temperatures than water, suburban and urban region which presents the highest mean LST.

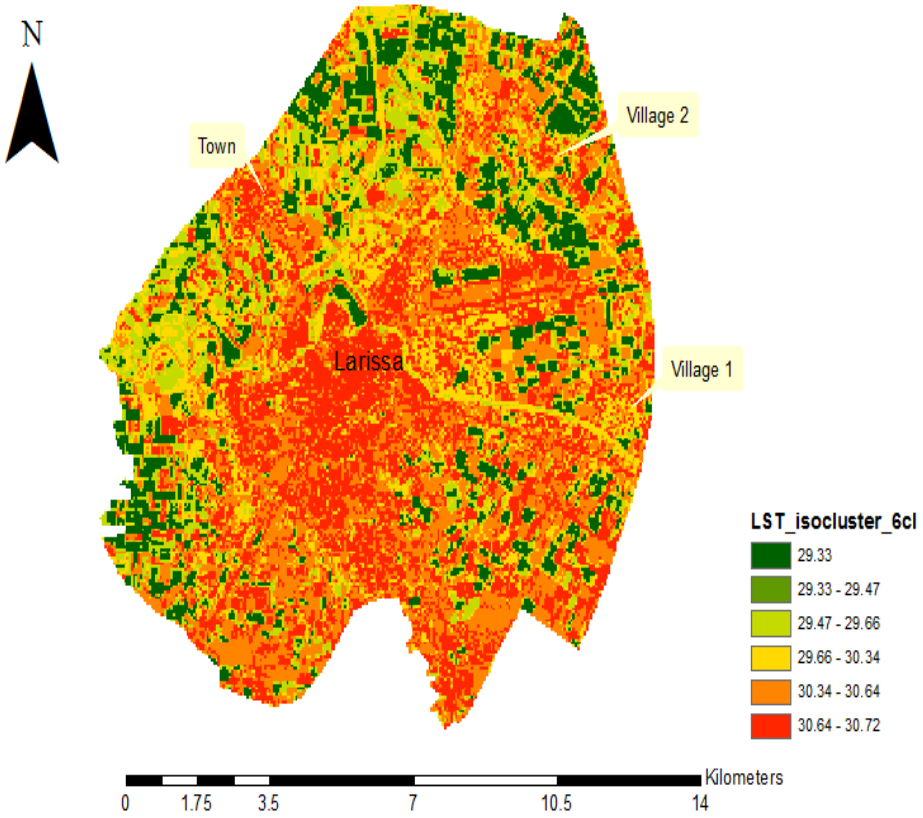

Figure 4.5: Mean LST values in Larissa region, at 01/08/2015.

Visual result of applying isocluster unsupervised classification method with 6 classes of LST in Larissa region, at 01/08/2015. The difference between mean LST of urban area and that of rural is approximately 1.4 °C, revealing the UHII.

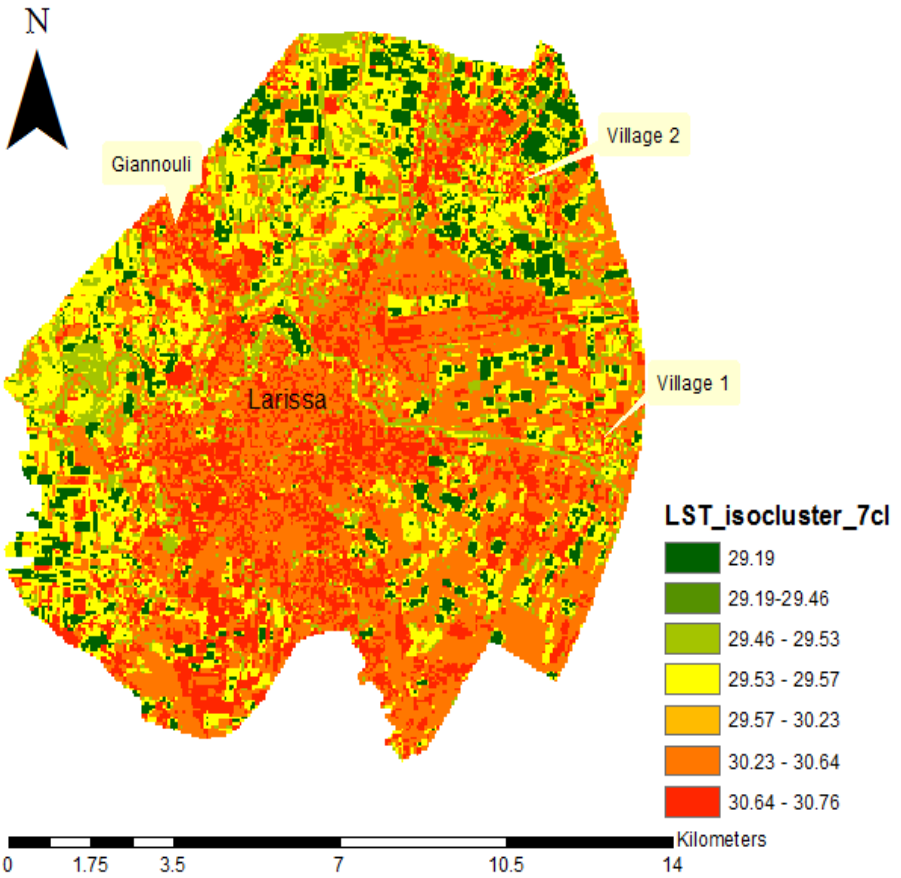

Figure 4.6: Mean LST values in Larissa region, at 01/08/2015. The isocluster unsupervised classification with 7 classes was applied.

In Fig. 4.6 the difference between mean LST of urban area and that of permanently irrigated land is approximately 1.6 °C, while the one between mean LST of urban area and that of non - irrigated land is approximately 1.3 °C. This approach reveals that the UHII between urban and rural area is estimated to lie between 1.3 and 1.6 °C.

The following two maps, Fig. 4.7, 4.8 reflect the UHII magnitude and pattern. Also, they reveal the inverse relation between LST and NDVI, related to mean values of the same classes. The urban area is the warmer and at the same time the lowest vegetated. Suburban and industrial/commercial regions are the second hottest and the second sparse vegetated. Urban vegetation holds the third place in mean LST, but it was found to be most vegetated, like the rural area. This proved to be the only exception, apart from water behavior, in the inverse relation among LST and NDVI.

The visual interpretation of the images, suggests that increasing vegetation abundance within urban and industrial/commercial areas might prove particularly effective in improving Larissa's climate. For the needs of this comparison, the class "

Suburban" that was used in calculating UHII, was splitted into two classes: " urban vegetation" and "Suburban/medium built". That is why, for the estimation of UHII, 6 classes were used while for the production of Fig. 4.8, 7 classes were utilized.

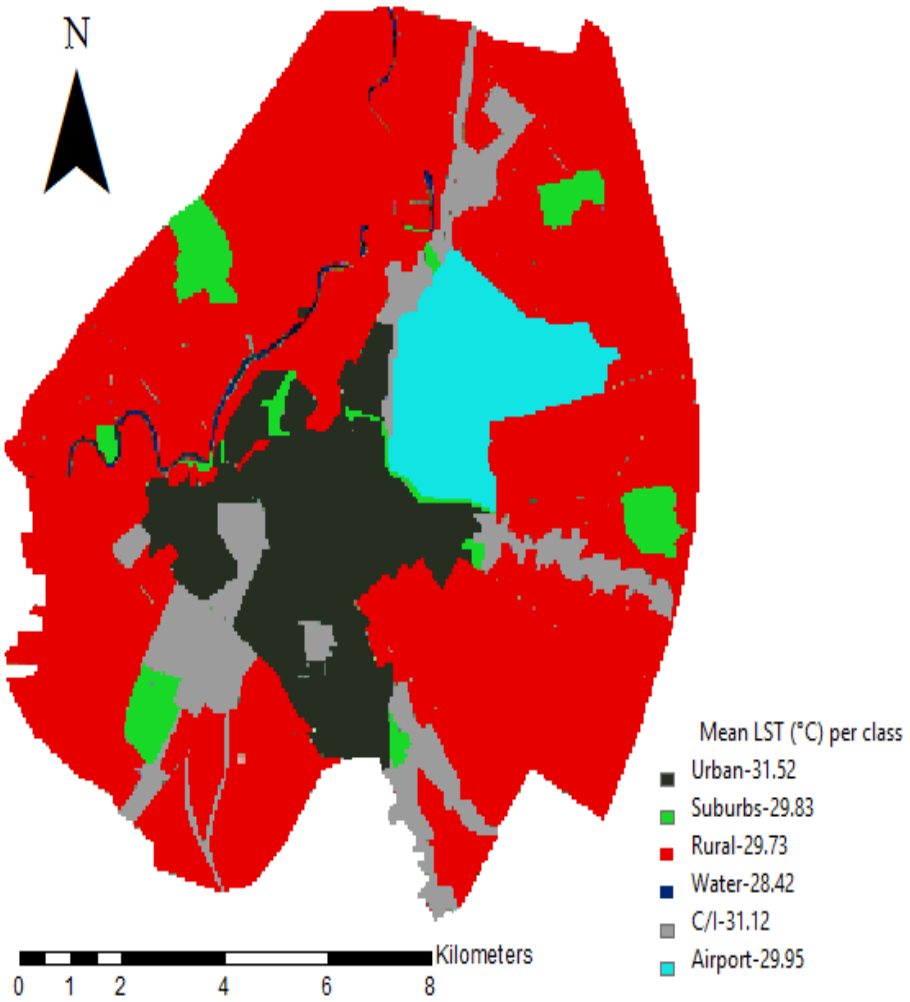

Figure 4.7: The spatial distribution of mean LST values for 6 different classes, after applying the polygon summary approach. The lower value of LST belongs to water, while the maximum one to urban area.

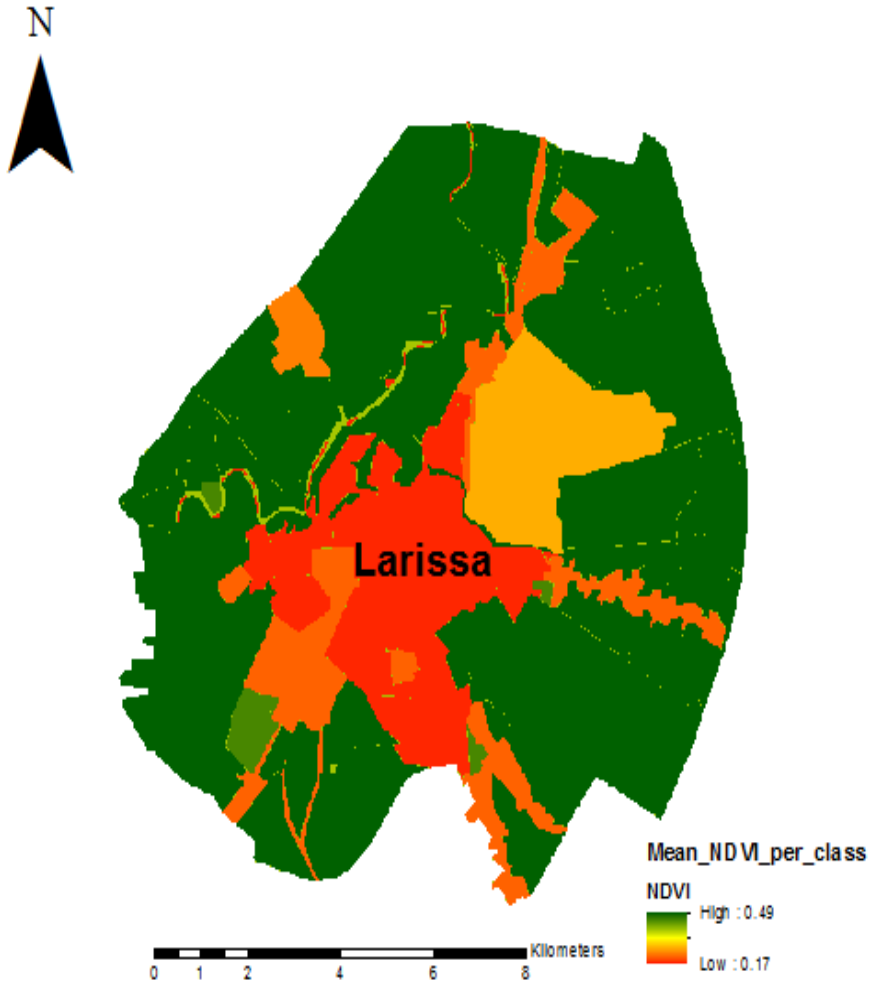

Figure 4.8: The spatial distribution of mean NDVI values for 7 different classes, after applying the polygon summary approach. The lower value of NDVI belongs to water and urban area, while the highest one to rural area and urban vegetation.

4.3 Strategies to reduce UHII

Relationship between urban surface temperature and land cover types help us to find out the best solution for urban environment quality improvement and the planning strategies for heat island reduction (Artis and Carnahan, 1982).Although urban climatologists have been studying urban heat islands for decades, community interest and concern regarding them has been more recent. This increased attention to heat-related environment and health issues has helped to advance the development of heat

island reduction strategies, mainly trees and vegetation, green roofs, and cool roofs. Interest in cool pavements has been growing, and an emerging body of research and pilot projects are helping scientists, engineers, and practitioners to better understand the interactions between pavements and the urban climate (EPA, 2014: Reducing Urban Heat Islands: Compendium of Strategies). According to "Cool Pavement Report" (EPA, 2015) permeable pavements may mitigate the impacts of increased urban water body temperatures due to UHII by percolating water through the pavement into subsurface storage areas where it can be dissipate through absorption and evaporation. Many communities have taken steps to reduce urban heat islands. Voluntary initiatives include demonstration projects, incentive programs, urban forestry efforts, weatherization programs, outreach and education, and awards to recognize and encourage heat island reduction activities. Policy initiatives include procurement, resolutions, tree and landscape ordinances, comprehensive plans and design guidelines, zoning codes, green building standards, building codes, and air quality standards.

The findings related to urban parks, show the importance of increasing vegetation cover and density, in order to decrease the UHI negative effects. According to a research in Athens in 2009, the combined presence of planting, water and shade is significant in the thermal comfort of civilians. The same study suggests that "flat tanks with cascade system" in a city park combined with shade also contributes greatly to the reduction of UHI negative effects. Other than water, a thorough study is necessary about other design elements, such as materials, planting, canopies, orientation of city parks, (greekarchitects.gr).

The interpretation of the study results about UHII denotes that increasing vegetation abundance within urban and industrial/commercial areas might prove particularly effective in improving Larissa's climate. In general, this study supports the above proposed strategies for the reduction of UHII.

5 CONCLUSIONS

According to Oke (1987), the UHII is reflected by the temperature differences between urban and rural sites and depends on the size, population and industrial development of a city, topography, physical layout, regional climate and meteorological conditions. The present study investigates the UHII in Larissa region, Greece, by means of satellite images, produced by L8 in the summer months of 2014, 2015 and about 12:00, at noon, local time. It suggests a widespread and easy to apply method, for the retrieval of LST in each pixel of an image - map.

The improved availability of satellite data having high temporal and spatial resolutions offers many opportunities. Thermal infrared images correlated with real-time meteorological stations temperature measurements permit the spatial distribution of LST to be modelled and estimated for an area of interest. Initially, this project examined the relationship between LST values, retrieved from L8 and temperature data measured by totally 16 different meteorological stations. The correlation results showed that measured temperatures and converted L8 LST values were in good agreement in the selected study area. Compared to similar studies, in other regions of Greece and elsewhere, the correlation coefficient between LST values and measured temperatures,

as well as the validity check of LST, were better than expected. This process was essential for the usage of LST in the estimation of UHII and the investigation of correlation with NDVI and VFC.

A correlation analysis between LST and NDVI, as long as LST and VFC, based on 01/08/2015 image, was conducted and it revealed that NDVI presents steeper slope in the correlation function and an increase of 0.1 in this index causes a decrease of approximately 0.572 °C in LST. In addition, an increase of 10% in VFC causes a decrease in LST values of approximately 0.568 °C.

Since NDVI is slightly easier to be retrieved, it may be more applicable to be under constant investigation, by means of satellites and ground research. In any case, an approximation in estimating LST values, through the knowledge of NDVI or/and VFC is supported and vice versa. Prerequisite for the sufficient estimation of one of the most important hydrometeorological variables, as Temperature, is the pre-processing and the reprocessing of the needed data. Especially, when referring to satellite data, this procedure is extremely important. All the steps that are described in Chapter 3 were followed cautiously, so as to derive the LSE and LST maps. 105 maps were produced by applying the above mentioned process in 7 images, in ArcMap 10.1 environment. The areas in the images that are less vegetated, like buildings, bare soil, water bodies as well as those that are characterised by dense vegetation, like mountain trees and agricultural areas could be easily detected.

The UHII examination in Larissa region contains the detection and estimation of the pattern and magnitude, respectively of UHII using 3 different approaches: Through a polygon ("zonal") summary approach, an unsupervised (Isocluster) and a supervised (ML) classification method. The investigation results revealed that the UHI ranges from 1.79 - 7.39 °C, according to first approach, but quite differently according to the classification approaches. This difference probably has to do with the fact that in the first method, the user defines precisely the boundaries of every area. In this way, there is no confusion if an amount of pixels is classified for example as rural or urban.

By using 6 classes, the ML - classification showed an UHII equal to 1.6 °C, and with Isocluster 1.4 °C. Applying 4 classes, the magnitude of UHII is decreasing to 1.25 and 1.3 °C. The greatest agreement is in the usage of 6 classes. In this case, the UHII is approximately 1.62 °C, and 1.6 °C by ML and Isocluster, respectively. The comparison of the results showed that the greatest similarity appears between ML-classification with 6 classes and the zonal summary technique, with the same number of classes.

In any case, all these three methods revealed the presence of UHI, its pattern and that land cover types, with the lowest values of vegetation cover and density, are characterised by high LST values. This study designates the impact of vegetation cover on the reduction of LST, and thus to the reduction of UHII and supports the importance of applying satellite data and the efficiency of satellite retrieved temperatures, in environmental related research field.

Interpreting thermal data and images of temperature distribution over an area is often not an easy job, because of many complex factors involved. The most influential factors for controlling the UHII are the distribution of surface cover characteristics, and urban morphology, such as building materials, geometry, and density. Each component surface in urban landscapes exhibits a unique radiative, thermal, moisture, and aerodynamic properties, and relates to their surrounding site environment. The tuple of

the component surfaces and the spatial complexity when they mosaicked create a limitless array of energy balance and microclimate systems, preventing urban meteorologists from drawing any generalization (Oke, 1982). This note reveals the complexity in the investigation of UHII.

In Larissa region a further research can be done so as to examine if and how the correlations between LST and NDVI depend on season of - year and time-of-day and also, if cooling effect of vegetation on LST is stronger during daytime than nighttime. The sufficient estimation of UHII and its causes in a region, such important as the Thessaly plain, is most helpful in policy making, related to environmental and thus social protection measurements. Taking this for granted and taking into account that Volos belongs to different climatic zone compared to Larissa, Trikala, Karditsa, a comparative examination of UHII would be of great interest.

Another perspective of this study is to be compared with other methodologies, concerning the retrieval of LSE and LST. Also, a thorough research in the relationship between LST and NDVI by LULC type in Thessaly can be conducted. Another general conclusion is that satellite thermal bands can be used for the creation of temperature profiles in large areas where the existence of meteorological stations is difficult. Thus, the retrieved LST values can be used in a future work, i.e: related to time series analysis of temperature values.

On the other hand, and as Stathopoulou and Cartalis note in their study in 2007 a disadvantage of the method may be considered the sun-synchronous orbit characteristic, the fact that the satellite passes over a place every 16 days and at a specific time. This limits the applicability of the method at a time other than the overpass time of the Landsat 8 satellite. However, despite this limitation, it is clear that this method can produce results that can be combined effectively with conventional field surveys for the integrated assessment of urban heat island.

REFERENCES

Ackerman, S., *Urban Heat Islands*, UW SSEC, 1985.

Akbari H., Potentials of urban heat island mitigation, International Conference:*"Passive and Low Energy Cooling for the built Environment"*, Santorini, Greece, 2005.

Aniello C., Morgan K., Busbey A., Newland L., Mapping micro-urban heat islands using Landsat TM and GIS, *Computers and Geosciences*, 21 (8), 965-969, 1995.

Arrau C.P., Pena M.A., The Urban Heat Island (UHI) Effect, October 2010.

Artis D. A., Carnahan W. H., Survey of Emissivity Variability in Thermoraphy of Urban Areas, *Remote Sensing of Environment*, 12, 313-329, 1982.

Boudas N., Investigation of urban heat island of Greek cities, *National Technical University of Athens*, 2014.

Carlson T. N., Ripley D. A., On the relation between NDVI, fractional vegetation cover, and leaf area index, *Remote Sensing of Environment*, 62, 241-252, 1997.

Chen, X.-L.; Zhao, H.-M.; Li, P.-X.; Yin, Z.-Y., Remote sensing image-based analysis of the relationship between urban heat island and land use/cover changes. *Remote Sensing of Environment*, 104, 133–146, 2006.

Dousset B., Gourmelon F., Satellite multi-sensor data analysis of urban surface temperatures and land cover, *Isprs Journal of Photogrammetry and Remote Sensing*, 58, (1-2), 43-54, 2003.

Farina A., Exploring the relationship between land surface temperature and vegetation abundance for urban heat island mitigation in Seville, Spain, *Department of Earth and Ecosystem Sciences*, Lund University, 2012.

Fortuniak K., Global environmental change and urban climate in Central European cities, *International Conference on Climate Change*, The environmental and socio-economic response in the southern Baltik region, Szczecin, Poland, 2009.

Gartland, L., Heat Islands: Understanding and Mitigating Heat in Urban Areas, UK & USA, *Earthscan*, 2008.

Giannaros T.M., Melas D., Daglis I.A., Keramitsoglou I., Kourtidis K., Numerical study of the urban heat island over Athens (Greece) with the WRF model. *Atmos. Environ. 73, 103–111*, 2013.

Giannopoulou K., Livada I., Santamouris M., Saliari M., Assimakopoulos M., Caouris Y.G., On the characteristics of the summer urban heat island in Athens, Greece. *Sustain. Cities Soc. 1, 16–28*, 2011.

Gill S. E., Handley J. F., Ennos A. R., Pauleit S., Adapting Cities for Climate Change: *The role of the Green Infrastructure Built Environment*, 33, 115-113, 2007.

Howard, L., The Climate of London (1833), *Meteorological Observations Made in the Metropolis and at Various Places Around it. London, Harvey and Darton cited in Gartland, L.*, 2008.

Hoyos Perez I. C., Comparison between Land Surface Temperature Retrieval Using Classification Based Emissivity and NDVI Based Emissivity, *International Journal of Recent Development in Engineering and Technology*, New York, 2014.

Jiménez-Muñoz J. C., Sobrino J. A., Gillespie A., Sabol D., Gustafson W. T., Improved land surface emissivities over agricultural areas using ASTER NDVI, Elsevier, *Remote Sensing of Environment* 103, 474-487, 2006.

Kalkstein L.S., A New Approach to Evaluate the Impact of Climate on Human Mortality, *Environmental Health Perspectives*, 96, 145-150, 1991.

Kassomenos P.A., Katsoulis B.D., Mesoscale and macroscale aspects of the morning urban heat island around Athens, Greece. *Meteorology and Atmospheric Physics 94, 209–218*, 2006.

Katsoulis, B., Theoharatos, G., Indications of the urban heat island in Athens, Greece. *J. Clim. Appl. Meteorol. 24, 1296– 1302*, 1985.

Liu K., Su H., Zhang L., Yang H., Zhang R., Li X., Analysis of the Urban Heat Island Effect in Shijiazhuang, China Using Satellite and Airborne Data, *International Journal of Remote Sensing*, 7, 4804-4833; doi:10.3390/rs70404804, 2015.

Livada I., Santamouris M., Niachou K., Papanikolaou N., Mihalakakou G., Determination of places in the great Athens area where the heat island effect is observed. *Theoretical Applied Climatology 71 (3-4), 219–230*, 2002.

Lo C. P., Quattrochi D. A., Land-use and land-cover change, urban heat island phenomenon, and health implications: A remote sensing approach, *Photogrammetric Engineering and Remote Sensing*, 69 (9), 1053-1063, 2003.

Mihalakakou P., Flocas H.A., Santamouris M., Helmis C.G., Application of neural networks to the simulation of the heat island over Athens, Greece, using synoptic types as a predictor. *J. Appl. Meteorol. 41 (5), 519–527*, 2002.

Mihalakakou G., Santamouris M., Papanikolaou N., Cartalis C., Tsangrassoulis A., Simulation of the urban heat island phenomenon in mediterranean climates. *Pure Appl. Geophys. 161, 429–451*, 2004.

Mitchell J. M., On the causes of instrumentally observed secular temperature trends, (1953), *Journal of Meteorology, 10:244-261*, cited in Gartland, L., 2008.

Mitchell J. M., The temperature of cities (1961), *Weatwise 14:224-229, 258* cited in Gartland, L., 2008.

Nichol J. E., A GIS-Based Approach to Microclimate Monitoring in Singapore's High-Rise Housing Estates, *Photogrammetric Engineering and Remote Sensing*, 60, 1225,-1232, 1994.

Oke T. R., Boundary layer climates, *Methuen Press*, London, pp. 252-302, 1987.

Oke T. R., The energetic basis of the urban heat island, *Quarterly Journal of the Royal Meteorological Society*, 108, 1-24, 1982.

Orhan O., Ekercin S., Dadaser-Celik F., Use of Landsat Land Surface Temperature and Vegetation Indices for Monitoring Drought in the Salt Lake Basin Area, Turkey, *The Scientific World Journal*, 142939, 2014.

Owen T. W., Carlson T. N., Gillies R. R., An assessment of satellite remotely-sensed land cover parameters in quantitatively describing the climatic effect of urbanization, *International Journal of Remote Sensing*, 19, 1663-1681, 1998.

Perakis K., Detection and prediction of diachronic land cover changes in the prefecture of Magnesia, with the application of Markov method and cellular automatic in multi-spectral satellite imagery, *Aeichoros*, 16:124-14, University of Thessaly publications, Volos, 2011.

Petropoulos G., and Carlson T.N., Retrievals of turbulent heat fluxes and soil moisture content by Remote Sensing. *Advances in Environmental Remote Sensing: Sensors, Algorithms, and Applications*, 2011.

Parry M. L., Canziani O. F., Palutikof J. P., van der Linden P. J., Hanson C. E., Contribution of working Group II to the Fourth assessment Report of the Intergovernmental Panel on Climate Change, *Cambridge University Press*, 2007.

Renou E., Differences de Temperature entre Paris et Choisy-le-Roi (1862), *Societe Meteorologie de France 10:105-109* cited in Gartland, L., 2008.

Renou E, Differences de temperature entre la ville et la champagne (1868), *Annuaire Societe Meteorologie de France 3:83-97* cited in Gartland, L., 2008.

Repapis C.C., Philandras C.M., Kalabokas P.D., Zerefos C.S., Is the last years abrupt warming in the national observatory of Athens records a climate change manifestation? *Global NEST J. 9 (2), 107–116*, 2007.

Roth M., Oke T. R., Emery W. J., Satellite derived urban heat islands from three coastal cities and the utilisation of such data in urban climatology, *International Journal of Remote Sensing*, 10, 1699-172, 1989.

Santamouris, M., Mihalakakou, G., Papanikolaou, N., Assimakopoulos, D.N., A neural network approach for modelling the heat island phenomenon in urban areas during the summer period. *Geophys. Res. Lett. 26 (3), 337–340*, 1999.

Santamouris M., Papanikolaou N., Livada I., Koronakis I., Georgakis C., Argiriou A. Assimakopoulos D., On the impact of urban climate on the energy consumption of buildings, *Solar Energy*, Volume 70, Issue 3, 201-216, 2001.

Santana L. M., Landsat ETM+ image applications to extract information for environmental planning in a Colombian city, *International Journal of Remote Sensing*, 28, 4225-4242, 2007.

Schmidt W., Zum Einfluss grosser Stadte auf das Klima (1917), *Naturwissen 5: 494-495* cited in Gartland, L., 2008.

Schmidt W., Die Verteilung der Minimum- temperature in der Frostnacht des 12 Mai 1927 im Gemeindegebiet von Wien (1929), *Fortschritte der Landwirtschaft 2 (21): 681-686* cited in Gartland, L., 2008.

Stathakis D., Land use classification using neural networks and remote sensing, PhD, Department of Planning and Regional Development, University of Thessaly, Volos 2003.

Stathakis D., How many hidden layers and nodes? *International Journal of Remote Sensing*, Volume 30, Issue 8, 2009.

Stathopoulou M., Cartalis C., Andritsos A., Assessing the thermal environment of major cities in Greece, International Conference: "*Passive and Low Energy Cooling for the Built Environment*", Santorini, Greece, 2005.

Stathopoulou M., Cartalis C., Daytime urban heat islands from Landsat ETM+ and Corine land cover data, Solar Energy, *Research Gate*, 2007.

Stathopoulou M., Synnefa A., Cartalis C., Santamouris M., Karlessi T., Akbari H., A surface heat island study of Athens using high-resolution satellite imagery and measurements of the optical and thermal properties of commonly used building and paving materials. *Int. J. Sustain. Energy 28 (1–3), 59–76*, 2009.

Stathopoulou M., Cartalis C., Mapping of urban heat island and index of quality of life for the city of Athens with combined using satellite images high timescale and GIS data, *National and Kapodistrian University of Athens*, 2011.

Sobrino J. A., Jiménez-Muñoz J. C., Paolini L., Land surface temperature retrieval form LANDSAT TM 5, Elsevier, *Remote Sensing of Environment*, 90, 434-440, 2004.

Streutker D. R., A remote sensing study of the urban heat island of Houston, Texas, *International Journal of Remote Sensing*, 23, 2595-2608, 2002.

Su W., Gu C., Yang C., Assessing the impact of land use/land cover on urban heat island pattern in Nanjing city, *China Journal of Urban Planning and Development*, 136, 365-372, 2010.

Sun, D., M. Kafatos, Note on the *NDVI-LST relationship and the use of temperature-related drought indices over North America, Geophys. Res. Lett., 34, L24406, doi:10.1029/2007GL031485*, 2007.

Voogt J. A., Oke T. R., Thermal remote sensing of urban climates, *Remote Sensing of Environment*, 86, 370-384, 2003.

Xian G., Crane M., An analysis of urban thermal characteristics and associated land cover in Tamba Bay and Las Vegas using Landsat satellite data, *Remote Sensing of Environment*, 104, 147-156, 2006.

Xue Y., Cracknell A. P., Operational bi-angle approach to retrieve the Earth surface albedo from AVHRR data in the visible band, *International Journal of Remote Sensing*, vol.16: 417-429, 1995.

Yu X., Guo X., Wu Z., Land Surface Temperature Retrieval from Landsat 8 TIRS-Comparison between Radiative Transfer Equation –Based Method, Split Window Algorithm and Single Channel Method, *Remote Sensing*, ISSN 2072-4292, 2014.

Yuan F., Bauer M.E., Comparison of impervious surface area and normalized difference vegetation index as indicators of surface urban heat island effects in Landsat imagery, *Remote Sensing of Environment*, 106, 375-386, 2007.

Yuan F., Bauer M. E., Comparison of impervious surface area and normalized difference vegetation index as indicators of surface urban heat island effects in Landsat imagery, Elsevier, *Remote Sensing of Environment*, 2006.

Yue W., Xu J., Tan W., Xu L., The relationship between land surface temperature and NDVI with remote sensing: application to Shanghai Landsat 7 ETM+data, *International Journal of Remote Sensing*, 28, 3205-3226, 2007.

Zisopoulou A., Kasdaglis M., Addressing the phenomenon of urban heat island through strategic planning of sustainable development of urban environment of Elliniko, 2011.

WEBPAGES

http://cimss.ssec.wisc.edu

http://en.climate-data.org

http://resources.arcgis.com

http://penteli.meteo.gr/stations

http://users.otenet.gr/~panaknik/Current-HistoryVantPro.htm

www.eea.europa.eu

www.e-meteolarissa.blogspot.gr

www.greekarchitects.gr

www.metar.gr

www.statistics.gr (Hellenic Statistical Authority)

www.wikipedia.org

landsat.usgs.gov/Landsat8_Using_Product.php

landsat.usgs.gov/calibration_notices.php

EPA, 2014

EPA, Reducing Urban Heat Islands: Compendium of Strategies-Urban Heat Island, 2009a.

EPA, Heat Island Effect, 2009b.

EPA, 2009a; WWF, 2010

US EPA, 2008.

APPENDIX A

Table A1: Meteorological Stations Information

Meteorological Stations	Altitude (m)	Coordinates		Land Type	Data provided by	Other characteristics
Agia station	167	39° 42' N	22° 48' E	Semi-urban	N.O.A	30 km. distance from Larissa city center
Sykourio private station	185	40° 15' 46" N	22° 58' 09" E	Rural	N.O.A & Mr. Grigoriou Vasileios	19 km. distance from Larissa city center
Karditsa station	91	39° 30' N	21° 54' E	Rural	N.O.A	6 km. distance from Karditsa city center
Larissa "6 dromoi" station	85	39° 38' 19" N	22° 24' 32"E	Urban	Mr. Douralis Ilias	0.9 km. distance from Larissa city center

Meteorological Stations	Altitude (m)	Coordinates		Land Type	Data provided by	Other characteristics
Larissa H.N.M.S station	72	39° 38' N	22° 27' E	Urban	H.N.M.S	3.9 km. distance from Larissa city center
Larissa "sifnou" station	82	39° 37' 39" N	22° 24' 50" E	Urban		1.3 km. distance from Larissa city center
Larissa "ATA" station	81	39° 38' N	22° 25' E	Urban	Mr. Panakoglou Vasileios	0.9 km. distance from Larissa city center
Larissa "Alexandros Takoudis"	82	39° 37' 39" N	22° 23' 55" E	Urban	N.O.A	2.2 km. distance from Larissa city center
Plastira Lake station	860	39° 15' N	21° 48' E	Rural	N.O.A	23 km. distance from Karditsa city center
Portaria station	600	39° 24' N	23° 00' E	Rural	Laboratory of Hydrology and Aquatic Systems Analysis, Civil Eng. Dep. - University of Thessaly & N.O.A	5 km. distance from Volos city center
Trikala station	163	39° 36' N	21° 49' E	Urban	N.O.A	0.5 km. distance from Trikala city center
Volos station	52	39° 24' N	23° 00' E	Urban	N.O.A & Dr. Spiliotopoulos Marios	1.8 km. distance from Volos city center
Volos private station 1	15	39° 21' 36" N	22° 56' E	Urban		1.4 km. distance from Volos city center

Meteorological Stations	Altitude (m)	Coordinates		Land Type	Data provided by	Other characteristics
Volos private station 2	30	39° 21' N	22° 56' 31" E	Urban		1.7 km. distance from Volos city center
Volos (UTH) station	9	39° 21' 36" N	22° 55' 54" E	Urban	Laboratory of Hydrology and Aquatic Systems Analysis, Civil Eng. Dep. - University of Thessaly & N.O.A	1.10 km. distance from Volos city center
Zagora station	505	39° 30' N	23° 06' E	Rural	N.O.A	15.8 km. distance from Volos city center

Table A2: Number of dates that each meteorological station participated in the correlation process.

Meteorological Stations	Correlation Dates
Agia - N.O.A station	4 out of 6
Sykourio -N.O.A (EAE) station	3 out of 6
Karditsa -N.O.A station	0 out of 6
Larissa-"6 dromoi" station	6 out of 6
Larissa- H.N.M.S (EMY) station	6 out of 6
Larissa-"sifnou" station	6 out of 6
Larissa-"ATA" station	6 out of 6
Larissa-N.O.A- "Alexandros Takoudis"	6 out of 6

Meteorological Stations	Correlation Dates
Plastira Lake -N.O.A station	0 out of 6
Portaria station-N.O.A station	1 out of 6
Trikala station	2 out of 6
Volos (N.E city center)-N.O.A station	2 out of 6
Volos (city center) private station 1	1 out of 6
Volos (city center) private station 2	1 out of 6
Volos (UTH)	1 out of 6
Zagora station- N.O.A station	2 out of 6

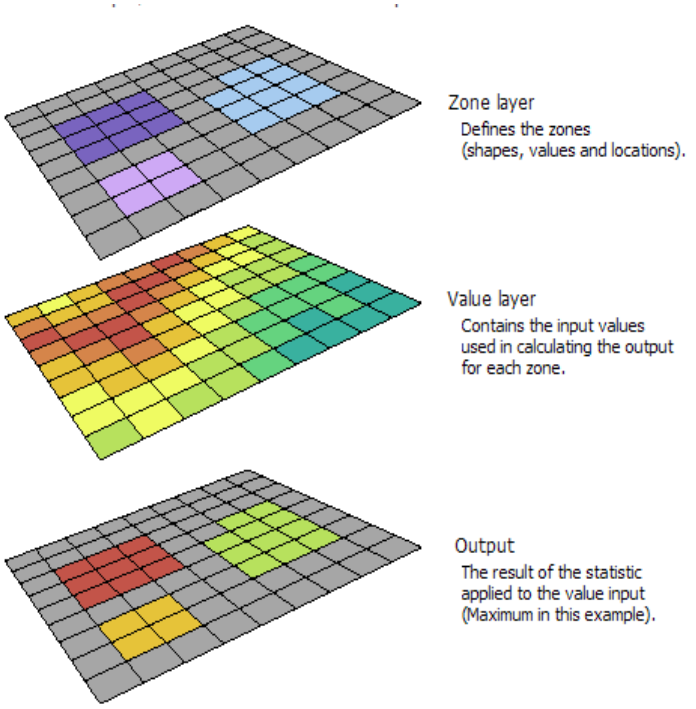

Figure A1. Illustrated example of how zonal statistics works (http://resources.arcgis.com).

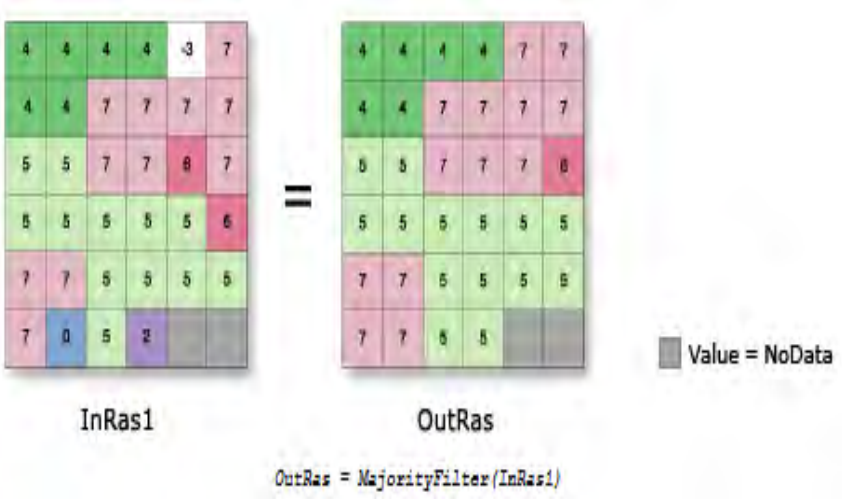

Figure A2. Majority Filter is applied to the input raster using a filter of the closest four cells (http://resources.arcgis.com).

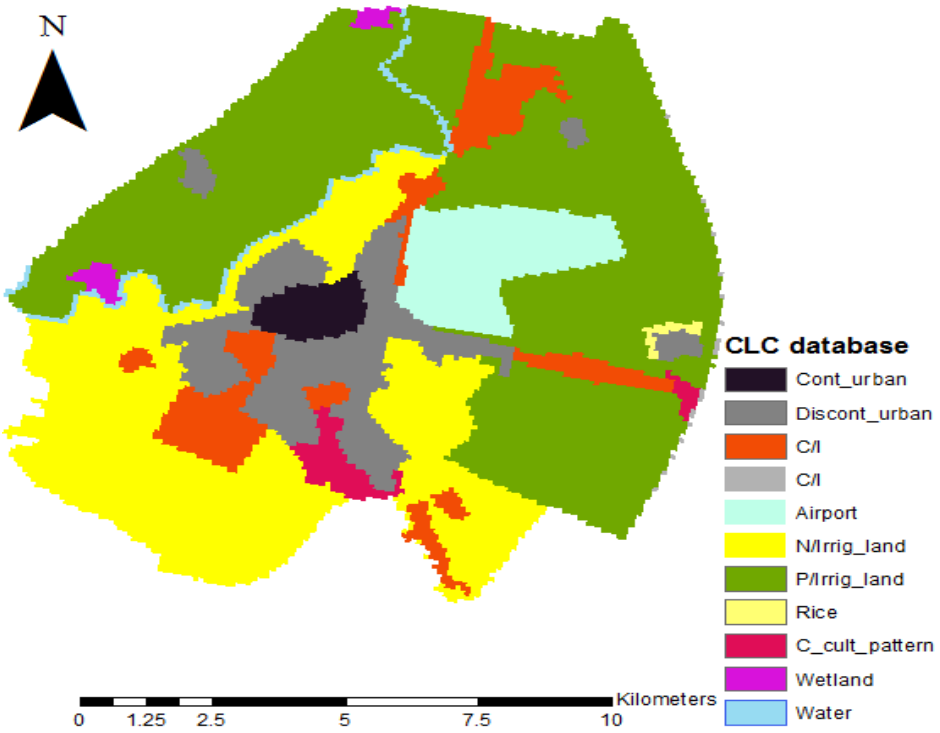

Figure A3: CLC 2000 database classification based on LULC types.

Training Sample Manager

ID	Class Name	Value	Color	Count
1	Rural	80		22824
2	Rural_Vegetation	23		132
3	Urban_Vegetation	17		154
4	Bare_soil	18		2171
5	Comm_Ind	32		3833
6	Urban	75		5314
7	Water	45		88
8	c_c_pattern	13		1965
9	Airport	5		3104
10	Parks	14		85
11	Suburbs	11		214

Figure A4: 11 initial classes based on LC polygons and CLC data base. Value stands for number of polygons, while Count for number of pixels (30 × 30 m^2).